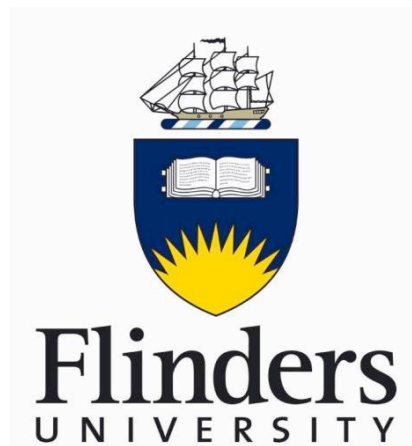# Investigation of Photodeposition of Gold on Titanium Dioxide Nanoparticles

Abdulrahman Alotabi

Supervisor
Prof Gunther Andersson

August 2017

Declaration

I certify that this thesis does not incorporate without acknowledgment any material previously submitted for a degree or diploma in any university; and that to the best of my knowledge and belief it does not contain any material previously published or written by another person except where due reference is made in the text.

………….……………………

Abdulrahman Alotabi

21/06/2017

Acknowledgements

Table of Contents

Abstract

In this work, we have investigated the photodeposition of gold (Au) on titanium dioxide (TiO_2) under different conditions. Nanoparticles of gold were prepared and loaded on titanium dioxide (TiO_2) using a method of photodeposition, and employed complementary techniques for example as X-ray Photoelectron Spectroscopy (XPS), Neutral Impact Collision Ion Scattering Spectroscopy (NICISS), UV photoelectron spectroscopy (UPS), and Scanning Electron Microscopy (SEM) to obtain information about the photodeposition properties of gold under a range of deposition conditions. Two types of gold were used in the study; (i) Chloroauric acid [$HAuCl_4$], and (ii) Au clusters [$Au_9 (PPh_3)_8$)] $(NO_3)_3$. The samples prepared were illuminated using UV light and radiation generated by a solar simulator to study the effect of spectral range of illumination sources. The $HAuCl_4$ had been pre-irradiated to study the effect of photo-reduction of $HAuCl_4$; employed pulsed and continuous irradiation techniques to study the effect of irradiation technique; varied the exposure time to study its effect; the effect of removing the phosphorus ligands from Au_9 by annealing, and lastly, varied the concentration of the samples to study the effect on the Au NPs and Au_9 clusters. It was found that it may the UV light activates both the Au compound and the TiO_2 faster than solar simulator to form Au NPs on the surface. Pre-irradiation and longer exposure times to UV light increases the amount of Au NPs deposited on the surface of TiO_2. At higher concentrations of chloroauric acid and Au clusters, more Au NPs are photodeposited on TiO_2. Under the effect of irradiation technique, it was found that more Au NPs are deposited on the surface of TiO_2 using pulsed technique than using continuous technique. It was also observed that heat treatment of Au_9 samples resulted to partial agglomeration leading to formation of larger Au particles except the lower concentration (0.001mM). They formed clusters on the surface.

1.0 INTRODUCTION

Over the last decades, nanoparticles and nanoclusters of noble metals supported on metal oxides have attracted a lot more interest due to their wide applications in heterogeneous catalysis [5]. According to Chusuei, et al. (2001), Gold (Au) in particular nanoclusters supported on Titanium dioxide (TiO_2) has the capability to catalyse some industrial reactions, such as partial oxidation of propylene to form propylene oxide and oxidation of carbon monoxide (CO). Au is chemically inert in its bulk form, but when deposited as nanoclusters on an oxide of a transition metal, its catalytic activity is greatly improved. Thus, nanoclusters reveal unique chemical and physical properties when their dimension is reduced to a few nanometers. These unique properties cannot be derived from those of bulk material [7]. Catalytic activity is strongly dependent on the size of the nanoclusters on the support [5].

Metal nanoparticles supported on a semiconductor surface of a metal oxide find applications in industrial photocatalysis processes, photocatalytic synthesis of solar fuel, purification, medicine, surface technology and waste water treatment [14]. According to Wenderich & Mul (2016), nanoparticles can significantly enhance the performance and stability of semiconductors in reactions that are stimulated by absorption of light energy. With suitable loading, cocalysts nanoparticles can function as (i) charge-carriers upon photoexcitation, repressing electron/hole recombination; (ii) active sties for reactions involving transfer of charges; and (iii) stimulated light absorption, particularly for gold and silver [14].

In this project, we will investigate the photodeposition of Au on TiO_2 nanoparticles to make an attempt to observe process conditions, particle size distribution, and oxidation states of the metals formed, among other observations.

1.1 Photodeposition

Photodeposition is a method used in the preparation of photocatalysts and metal-supported catalysts. It is a phenomena where illumination of a slurry of particles of a semiconductor in an aqueous phase solution, leads to deposition of well-defined nanoparticles of metal oxide on the surface of the semiconductor [14]. Generalized equations of reductive and oxidative photodeposition for a metal M is as follows:

Oxidative photodeposition:

M^{n+} *(aq) + ne⁻* $\longrightarrow$ M*(s)*

Reductive Photodeposition:

M^{n+} *(aq) + nh⁺+ n*H_2O $\longrightarrow$ MO_n*(s) + 2n*H^+ [14].
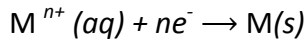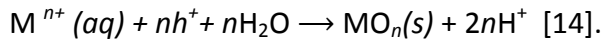
Thus, photodeposition is based on light-induced electro-chemistry and involves oxidative and reductive photodeposition as shown in figure 1 below.
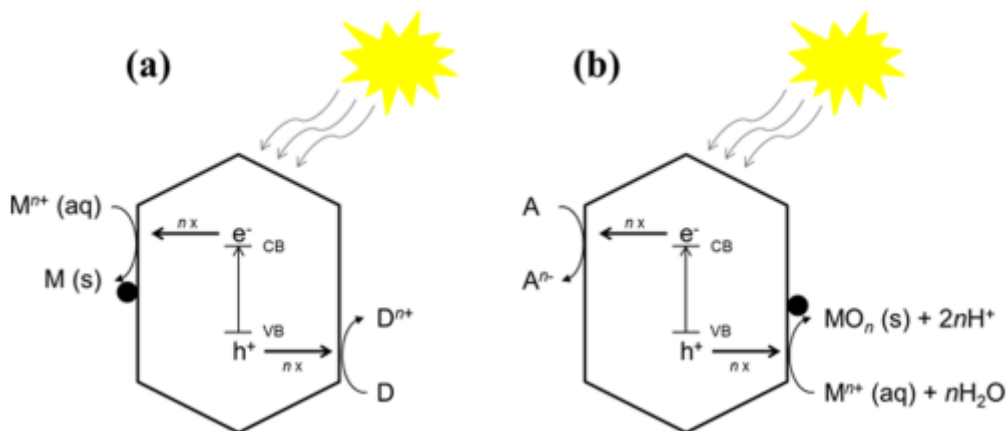
Figure 1: Schematic illustration of (a) reductive and (b) oxidative photodeposition [14]. CB – conduction band; D – electron donor, M – metal; VB – valence band; A – electron acceptor; VB – valence band; n – number of electron-holes.

The irradiation of metal oxide powder with UV light causes reduction of metal cations with appropriate redox potential from the photo-excited electrons. This creates metal particles on the surface of the metal oxide. The way in which adsorption takes place and the efficiency of charge separation; in turn influence the photocatalytic activity of the material [11].

1.2 Photocatalysis

Photocatalysis is the process in which light energy is converted into chemical energy. For this process to occur, a material that can provide a temporary state decay to form some chemical species when irradiated with light is required. Semiconductor metal oxides, such as ZnO and TiO_2 are typically used as photocatalysts [12]. Upon light absorption, charge

separation occurs with the formation of an electron in the conduction band and an electron hole in the valence band [12]. The pair of electron-hole created may recombine and then is lost or separate to form independent pairs of electron-holes and allow the transfer of charge between the electron-hole pairs and the reactants on the surface of the TiO_2 semiconductor [2]. At this stage, photo-excitation takes place. In TiO_2, electrons diffuse faster in the conduction band while hole-migration occurs by charge-jumping from neighbouring sites. In heterogenous photocatalysis, photo-induced reactions occur at the surface of the catalyst [9]. Titanium dioxide has been widely used as a photocatalyst in a series of oxidative and reductive reactions on the surface of the semiconductor. This is largely contributed by the existence of lone electron in its outer orbital [4].

Electron and holes that fail to be annihilated move to the particle surface where they can react with other chemical species [12]. UV light is commonly used in the photo-excitation process to reduce the metal onto the surface of the metal oxide, activating the metal oxide. UV light excites valence band electrons to the conduction band of the semiconductor, creating holes in the valence band. Figure 2 shows a schematic diagram of this process and the reactions involved.

O – Oxidation;

R - reduction.

The process of TiO_2 activation under UV light can be represented by the equation:

$TiO_2 + hv \rightarrow h^+ + e^-$
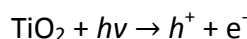
In this reaction, h^+ is a powerful oxidizing agent, while e^- is a powerful reducing agent [6]. The oxidative and reactive reactions are as follows:
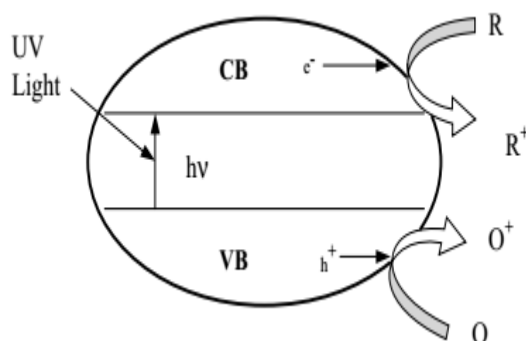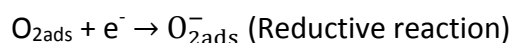
Figure 2: A schematic diagram of the photo-excitation process of TiO_2 as a

$OH^- + h^+ \rightarrow OH$ (Oxidative reaction)

$O_{2ads} + e^- \rightarrow O_{2ads}^-$ (Reductive reaction)

1.3 Catalytic Activity of Gold

In its bulk nature, gold (Au) is considered as an inert material. However, Au nanoparticles (Au NPS) and Au nanoclusters with nanoscale dimensions have unique catalytic properties that can modify surfaces due to their specific physical, chemical composition and crystal structure [10]. When Au particles and Au clusters are supported on the surfaces of substrates for example TiO_2, the resulting hybrid nanomaterial can be used to catalyze important industrial reactions which depend on the size of the nanoscale gold.

Gold Nanoparticles as co-catalytic

The Au particles provide a larger surface area between the reacting material and the active catalytic material, which enhances the catalytic reaction process. Au NPs have a face-centered cubic structure with a continuous energy band structure that resembles that of bulk material [22]. Au NPs exhibit a strong absorption of visible light in the optical spectrum due to plasmonic effects at the surface and is known as surface plasmon resonance (SPR). The intense colour of Au NPs larger than 3 nm is as a result of this feature. The plasmon band is highly sensitive to the particle size and its intensity reduces with decrease in the core size due to quantum size effects and loss of metallic property. The small size of Au NPs increases the dispersion, and subsequently, the number of edges and kinks on the metallic properties, which leads to stabilization of high index facets [10].

Gold Nanoclusters as co-catalytic

Gold nanoclusters (Au NCs) are smaller than Au NPs, typically less than 3 nm and can also dramatically modify surface properties. As opposed to the crystal structure in Au NPs, it is the geometric fluxionality and the size-dependent electronic structure that are important for surface modification properties of the Au NCs. Au clusters form specific atomic structures that are dependent on the number of atoms in the NCs. Addition or removal of a one atom in a cluster can have a complete alteration of the catalytic activity of the material [8]. Thus, the number of atoms in an Au cluster has a strong influence on the
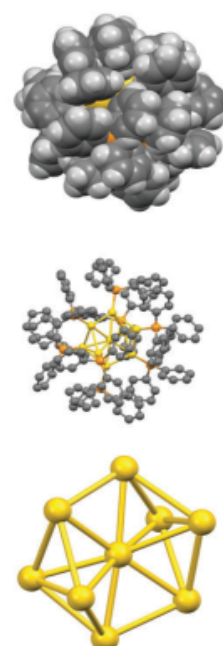
4

Figure 3: An overview of the

catalytic properties of the modified surfaces, which also depend on the size, electronic structure and morphology of the Au NCs [22].

Clusters are used due to the following reasons:

i. They have specific electronic states, as opposed to a band.

ii. They exhibit fluxionality and structural isomerism, features that allow easy change between configurations, helping with attachment and detachment of molecules.

iii. They also exhibit a larger surface area relative to the amount of material used and could also change the surface of the electronic semiconductor. However, this has not been clearly demonstrated.

1.4 TiO$_2$ as Photocatalyst material

Titanium dioxide is widely applied as a photocatalyst due to its excellent properties: (i) it has high catalytic efficiency, very stable, durable, safe and inexpensive; (ii) does not require chemical additives; (iii) promotes oxidation of pollutants at ambient temperature; and (iv) can completely degrade a wide range of pollutants at certain operation conditions [15]. Durability and stability under irradiation is one of the prerequisites of a photocatalyst. For this reason, chalcogenides and metal sulphide are not used as photocatalysts even though these materials exhibit a high catalytic activity [12]. They also tend to exhibit photocorrosion and dissolve under irradiation in aqueous phase [12]. Some researchers have demonstrated that TiO$_2$ film has a higher catalytic activity compared to the most active TiO$_2$ powder [15]. Furthermore, TiO$_2$ is very robust with high photochemical activity, available and affordable, and does not have toxicity, thus making it the most used photocatalytic material.

Titanium dioxide has two crystal phases: rutile and anatase. Anatase, which had been used in this project, is more superior to rutile for photocatalytic application [15]. This is because the location of the conduction band of anatase is more suitable for activating conjugate reactions that involve electrons. Furthermore, during a photo-oxidation reaction, the surface peroxide groups formed at anatase are very stable as opposed to those formed at the surface of rutile [15].

2.0 Project objectives

Photodeposition method was used to deposit Au on TiO_2. The goal of this research study was to investigate the effect and control of experimental conditions on the rate of photodeposition of gold onto the surface of TiO_2 and the size of Au particles formed via photodeposition. The changes in the structure and characteristics of chemically synthesized Au NPs and Au cluster deposited on the surface of TiO_2 depend on many parameters, including irradiation time, irradiation source, concentration value of prepared solution, irradiation technique etc. In this project, we used two types of gold; $HAuCl_4$ and Au_9. The main objectives of the project were to:

I. Understand correlation between the conditions of irradiation and the amount of Au deposited and the size of the particles and their chemical state. All conditions have been listed below:-

1. Gold (III) chloride hydrate ($HAuCl_4$) or Gold cluster [Au_9 ($PPh_3)_8$)] ($NO_3)_3$ have been used.
2. Samples irradiated by UV light or sunlight spectrum.
3. Time of exposure.
4. Irradiation technique (Pulsed and Continuous)
5. Varying concentrations.
6. Heat treatment of Au_9 to remove the phosphors ligands.

Characterization of the NPs produced were analysed using methods such as XPS, NICISS, UPS and SEM.

3.0 Experimental section

Materials

The Materials that had been used in this project are Si (100) wafer as a substrate and TiO_2 paste (DSL 18NR-T Dyesol)"Anatase NPs". Also, Gold (III) chloride hydrate ($HAuCl_4$) was purchased from ALDRICH and Gold Cluster [Au_9 ($PPh_3)_8$)] ($NO_3)_3$. Two solvents have been used; ethanol and methanol.

Models and Specifications of light sources

There were two different illumination sources used. The first; UV LED (362.5nm to 370nm). The power and intensity fallen on the sample were roughly equivalent to 690 mW and 65

angle of half intensity. The distance from UV lamp to the sample is 1 cm and the area of the sample is 1 cm^2 by calculate the intensity ~ 109 mW/cm^2. The UV radiation in angle of 180 so the power and intensity that hitting the sample estimate to be 345 mW and 54 mW/cm^2. The second illumination source is solar simulator (300W Xenon) the power of was 300W and the total intensity was 147 mW/cm².

Photodeposition of Au Nanoparticles.

TiO$_2$ films were prepared by spreading a TiO$_2$ paste onto 1.1mm×1.1mm Si (100) wafer using the doctor blade method, followed by heat-treating at 450 °C for 30 minutes. The thickness of the TiO$_2$ films, determined from using the scanning electron microscopic (SEM) images, was ~ 4 µm. The HAuCl$_4$ solutions prepared in ethanol with concentration of (0.1375 mM).

The Photodeposition of HAuCl$_4$ on TiO$_2$ were conducted in three steps. First, preirradiation (preirradiation of HAuCl$_4$ increase the photodeposition rate [18]) of 1.8mL of HAuCl$_4$ solution for 6 minutes and then the TiO$_2$ sample placed on the solution. After that, the sample irradiated for 20 seconds. There were two irradiation techniques that were used to irradiate the samples. The first technique was the "pulsed" technique, where can be generated spherical Au NPs [18], 4 x 5 seconds exposure to light with a 30-seconds gap between pulses. Therefore, with this technique, the overall exposure time was 20 seconds. The second technique was the "continuous" technique, where can be generated Au clusters [18], in which the samples were exposed to light for 20 seconds. The average time that a sample spent on the solutions was ~ 70 seconds for continuous technique and ~110 seconds, including the photodeposition time. The investigation had done for various illumination times (10s, 20s, 30s, 40s, and 50s) and different concentrations (0.1mM, 0.05mM, 0.01mM, 0.005mM, 0.001mM, 0.0005mM, and 0.0001mM).

Photodeposition of Au Clusters

Here, TiO$_2$ was prepared in the same way that been explained before. Solutions of Au$_9$ were always prepared in methanol. **The Photodeposition steps:** first, placed the TiO$_2$ sample in 1.8mL of Au$_9$ solution then irradiated the sample with UV light for a single continuous exposure. The average time that a sample spends on the solutions was ~ 60 seconds, including the photodeposition time. Different exposure times had been investigated (10s, 20s, 30s, and 40s) with different concentrations (0.1mM, 0.01mM, and 0.001mM).

Moreover, heat treatment at 200C for 10minutes had done for 10s and 20s with different concentrations (0.1mM, 0.01mM, and 0.001mM) to remove the phosphors legions

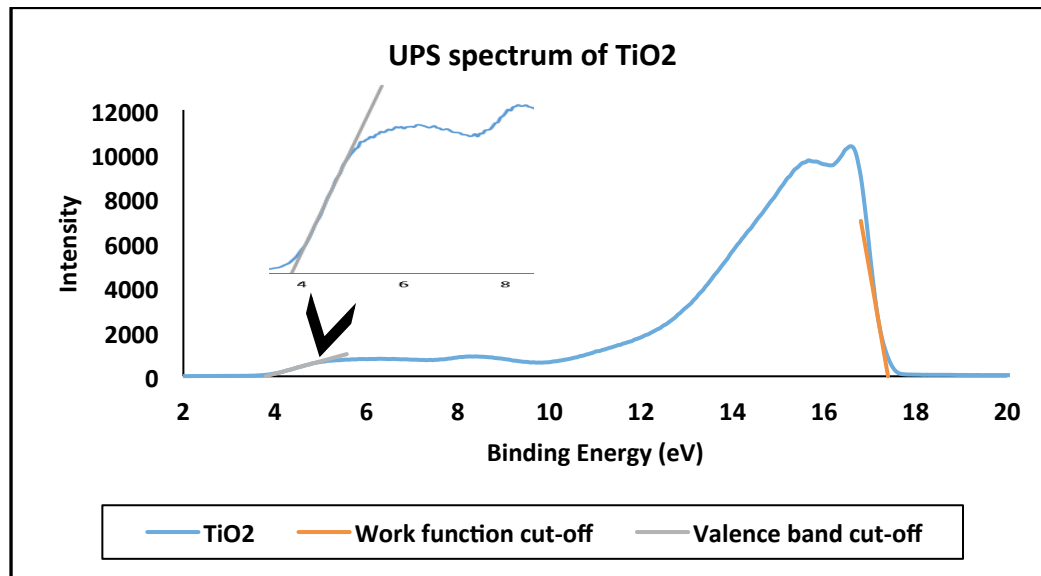**Determine the valence band and work function from UPS Spectra of TiO$_2$**

Figure 4: The UPS spectra of TiO$_2$ in the valence band and work function regions

In UPS, the work function is measured from the lowest kinetic energy electrons that escape from the surface of a sample. Work function of TiO$_2$ can be determined from the UPS shown in figure 4, since the binding energy of the electrons at the secondary edge (work function cut-off) is known. It is given by determining the difference between the energy of the UV photons and the binding energy at the secondary edge. From our UPS spectrum in figure 4, the investigated TiO$_2$ surface has a binding energy of 17.4 eV at the secondary edge, using (He I) irradiation with UV photon energy of 21.2 eV. Hence, it follows that the work function (Φ) is given by:

Work function = UV photon energy – (Binding energy at the secondary edge cut-off)

$$\Phi TiO_2 = 21.2 \text{ eV} – 17.4 \text{ eV} = 3.8 \text{ eV}$$

The work function cut-off of the UPS defines the work function since it represents the secondary electrons at the surface of TiO$_2$ sample which had just sufficient energy to

overcome the work function. The He I irradiation has the capability to ionize electrons from the valence levels which form the outermost levels of element atoms [34].

4.0 Analytical Techniques

4.1 X-ray Photoelectron Spectroscopy (XPS)

XPS surface analysis is performed by irradiating a sample using monoenergetic soft X-rays of sufficient energy and detecting the emitted electrons [26]. The x-rays can be from sources of radiation with usually excitation energy of 1253.6 eV for Mg Kα or 1486.7 eV for Al Kα. When a beam of an x-ray hits the sample, the electrons in the sample undergo excitation. The X-ray photons excite electrons that produced after excitation interact with the atoms on the sample surface, resulting in emission of electrons due to the photoelectric effect. Hence, XPS signal is exponentially surface sensitive because only the electrons that are ejected from the surface are detected. The average distance moved by an electron through a solid before energy loss is called electron mean free path. Once in the vacuum, the electrons are collected by an electron analyser which measures the kinetic energy of the electrons. The kinetic energy of the emitted electron can be measured by this equation:

$$KE = hv - BE - \phi s$$

The hv is the energy of the photon, BE is the binding energy of the atomic orbital from which the electron originates and ϕs is the spectrometer work function (constant) [26].Figure 5 shows a schematic representation of XPS.
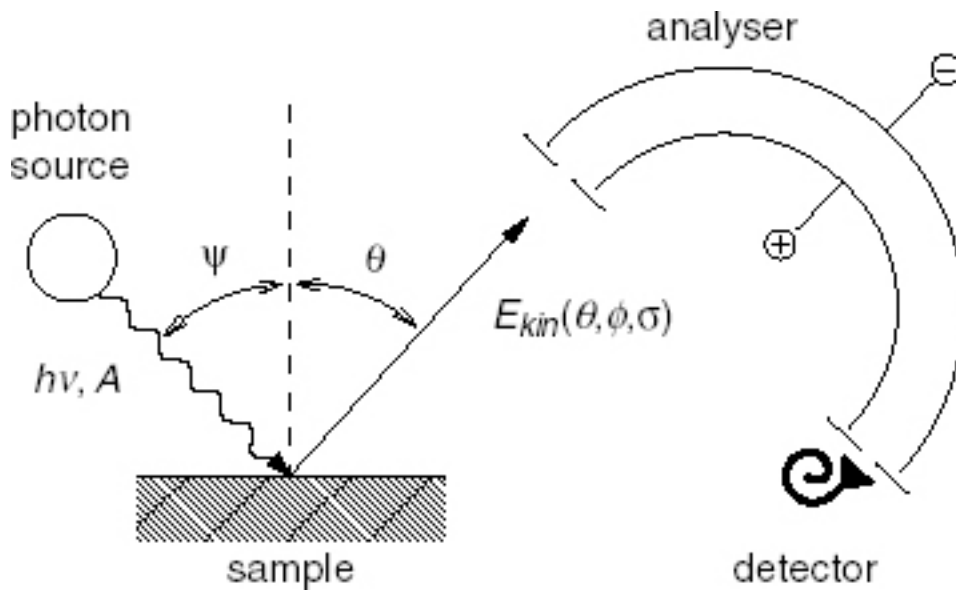
Figure 5: Principle of a photoemission spectrometer. Monochromatic photons with energy hv=1486.7 eV are produced by a light source and hit the sample surface under an angle Ψ with respect to the surface normal. The whole setup is evacuated to ultra-high vacuum. (*Source*: [38])

An electron analyser produces a spectrum of electron intensity versus binding energy with energy peaks that correspond to a particular element present in a sample. The chemical composition of a specimen is obtained by determining the respective contribution by every peak area [30]. The actual binding energy of an electron is not only dependent on the level of occurrence of photoemission and chemical bonding in an element, but also on the local physical and chemical environment, and formal oxidation state of an atom. A change in these factors produces chemical shifts in the peak positions in the XPS spectrum. The chemical state of the specimen being analysed can be determined using chemical shifts. The sample sometime acquire a steady-state charging during the scan and that will shift the XPS peaks to the higher binding energy so the calibration is required. It needs to use C 1s photoelectron peak at 285 eV to calibrate the energy scale for all spectra [26]. The initial and final effects determine the peak position as well as the FWHM, which are influenced by the elements present in the clusters, the particle size of these elements and the interaction between the clusters and the substrate. The initial state effect provide information about the chemical state of an atom near the surface which can help to determine the oxidation state of $HAuCl_4$ [40]. In the final state effect, the atom excited by absorption of photons undergoes de-excitation process. After excitation, the nano-clusters of gold can stay in a

10

charged state for some time depending on the size of clusters and the type of substrate. So, the peak position and width provide important information to understanding the electronic structure of clusters [16].

In our project, we used XPS to provide the information on surface composition and chemical states which would help to study the effect of photodeposition of $HAuCl_4$ and Au_9 onto TiO_2. Moreover, XPS used to study the oxidation of $HAuCl_4$ and determine the size of Au clusters before and after heating. Also, we monitored the organic ligands that may present on the surface for Au_9.

4.2 UV photoelectron spectroscopy (UPS)

UPS is similar to XPS in terms of the principle of operation, with the only difference being that in UPS, the photoelectric effect is induced using ionization radiation at energies in the range of 0-100 eV, while in XPS photon energy > 1000 eV are usually used [25]. At lower excitation energies we can determine the valence electron and at higher excitation energies the core electrons.

In this project, UPS was applied to determine the valence band structure and the work function of the Au NPs and Au clusters after deposited onto the TiO2 by photodeposition method. This accomplished by irradiation the Au/TiO2 samples with UV photons from helium gas with energies of 21.2 eV (He I) in order to obtain the binding energy.

4.3 Neutral Impact Collision Ion Scattering Spectroscopy (NICISS)

NICISS typically involves directing a pulsed beam of inert gas ions, preferably helium ions, (He+) at low energy ($\approx$ 3 keV) onto a sample [29]. As the ions travel to the sample surface, they become neutralized and continue travelling through the sample until they collide with an atom, then are backscattered. The backscatter ions are detected by micro-channel plates to produce time-of-flight (TOF) spectrum. The energy of the backscattered projectiles is determined by their TOF from the target atom to the detector. During the backscattering process, the projectiles lose energy in amount proportional to the mass of the element on target. As the ions penetrate through a sample, there is continuous energy loss consisting of electronic excitations and small angle scattering [29]. In analysing data from NICISS spectrum, there are two ways to consider the inelastic energy. First, inelastic energy loss has

to be considered for determining the energy of the backscattered projectile. Second, the inelastic energy loss due to small angle scattering forms part of the continuous energy loss of the projectiles that pass through the material and depends on the energy loss straggling and stopping power of the section.

The TOF spectrum is an energy loss spectrum that can be used to provide information on the composition, the crystalline structure, and the concentration depth profiles of elements (in non-crystalline samples) on the surface or near-surface regions of a material when projectile ions interact with a target atom in matter [28].

NICISS used in this project investigated the concentration depth profiles of Au NPs (from $HAuCl_4$) and Au clusters (from Au_9) that deposited on the surface of the TiO_2 using photodeposition method. This information is essential to understand the crystal structure and orientation of the hybrid surface

4.4 Scanning Electron Microscopy (SEM)

Unlike the other methods, SEM has the capability to image and analyse bulk material. SEM operates on the principle illustrated in figure 6. The technique uses a beam of electrons to produce an image of a material under investigation, and magnifies the image by electromagnetic fields. A typical SEM machine consists of a component called the gun, which generates the electrons, a series of lenses for focussing and shaping the beam of electrons, a sample holding chamber, and pumps that maintain a vacuum environment for imaging.

Electrons from a field emission cathode, a thermionic, or a Schottky cathode in the gun are accelerated through a cathode and an anode with a voltage difference in the range of 0.1 keV – 50 keV. Low-voltage SEM ranges from 0.1-5 keV, while high voltage SEM ranges from above 5 – 50 keV [27]. The accelerated beam of electrons is focused over the surface of the material on the sample chamber in order to create an image. The beam of electrons is raster scanned on the sample surface, and the position of the beam is combined with the signals detected to form an image. As the electrons in the beam interact with the sample, secondary electrons and other radiations are produced from the surface of the sample. The secondary electrons are collected by a detector which converts them into signals, which are scanned using a television system to create an image on a cathode ray tube; and their

number depends on the surface topography. The image produced can be used to obtain information on the sample surface composition, distribution of various elements in the sample, surface topography, and mineral orientation.
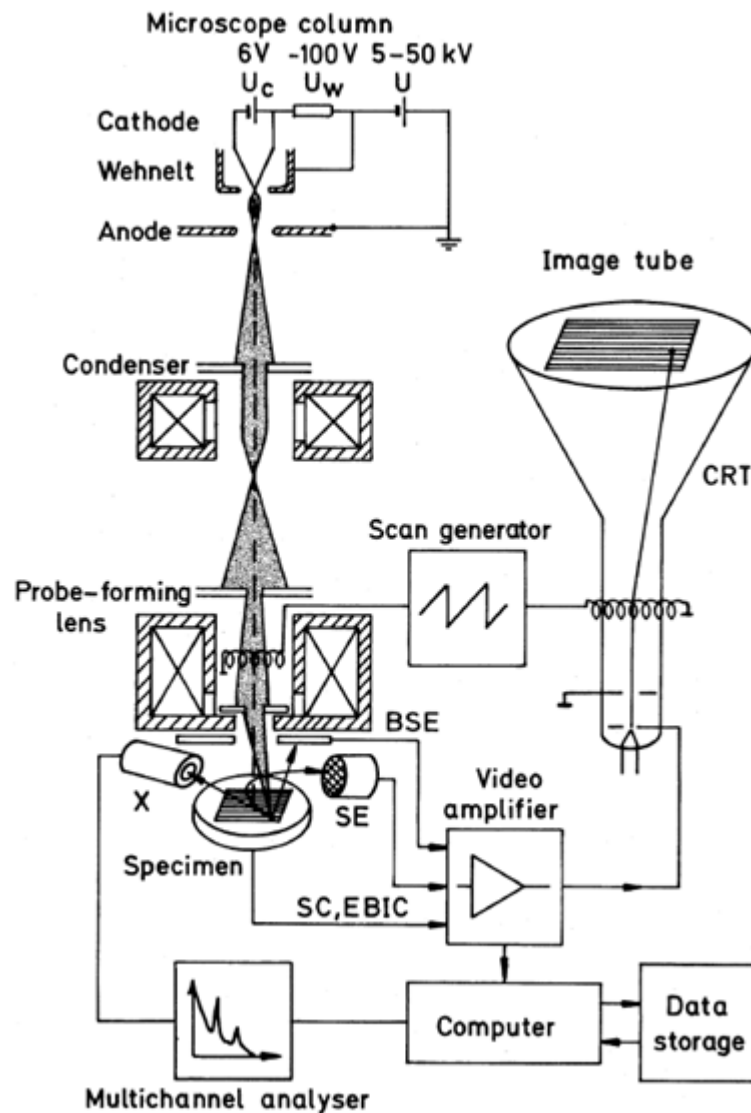

Figure 6: Working principle Of SEM (SE – secondary electrons; BSE – backscattered electrons; EBIC -electron beam-induced current; SC – specimen current; CRT – cathode ray tube; X – x-rays). *Source*: [27].

Thus, SEM technique used confirms the elemental composition and distribution of elements, as well as the surface topography of the Au NPs that deposited in the surface of the TiO_2.

5.0 Results and Discussion

5.1   Photoreduction of Chloroauric acid [HAuCl$_4$]

For XPS results, it is important to note that the change on the peak position of the Au for HAuCl$_4$ related to chemical states of the Au.

Photolysis of AuCl$_4^-$ produces AuCl$_3^-$ and a radical chlorine species that is highly reactive. The AuCl$_3^-$ disproportionate rapidly to regenerate AuCl$_4^-$ and produce AuCl$_2^-$, which is a metastable intermediate that can further undergo slow disproportion to give Au^0[18]. Then, Au^0 nucleate and grow into Au NPs. Furthermore, alcohols (for example Ethanol) can be used to generate a powerful reducing free Cl radical that by abstract hydrogen. Basically, irradiation of HAuCl$_4$ solution reduce Au(lll) to Au(l) and then to gold atoms Au^0 and then atoms can growth to form Au NPs.

$$Au(lll) \xrightarrow{hv} Au(l) \xrightarrow{hv} Au^0 \qquad (1)$$
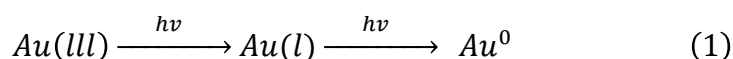
In this project, we used XPS to study the effect of photoreduction of HAuCl$_4$. The reference sample of HAuCl$_4$ prepared by drop casting HAuCl$_4$ on TiO$_2$ sample in the dark and then measure it in XPS. The Au peaks can be seen on the figure 7 (a) below.
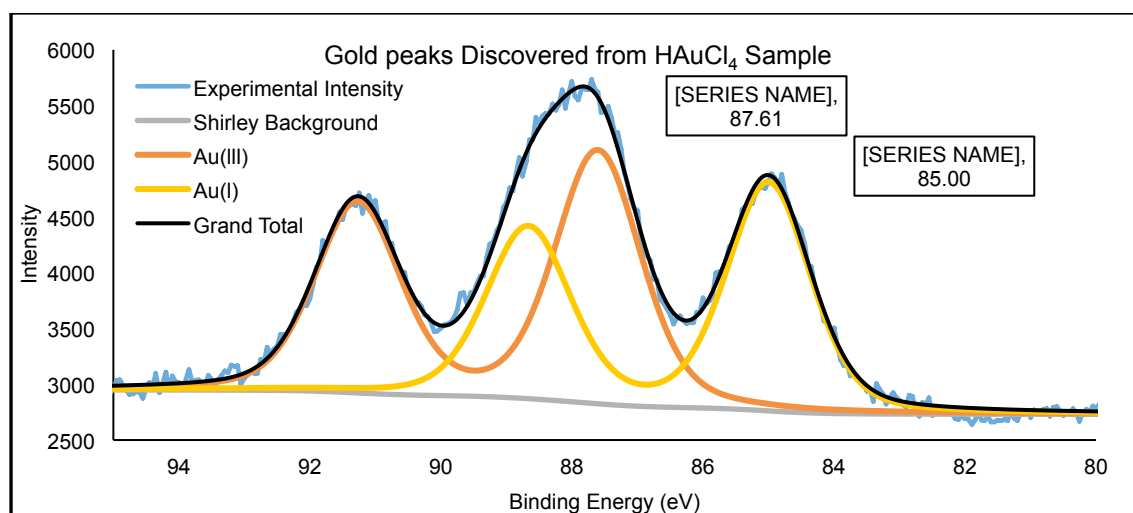

Figure 7(a): XPS Results of Chloroauric acid [HAuCl$_4$].

From figure 7(a), gold has two double peaks separated by 3.67 eV, first peak 4f$_{7/2}$ (at the lower binding energy) second peak 4f$_{5/2}$ (at the higher binding energy), spin-split effect. We assume that first peak at 85 eV corresponding to Au(l) and the second peak at 87.61 eV to

14

Au(lll)[39]. This scan took 7 to 8 minutes and following the scan, was through surveyed, titanium, carbon, oxygen, and silicon. That took around 30 minutes then I scanned for gold a second time. The spectra in figure 7(b) show the second scan of gold after ~ 30 minutes exposure by XPS.
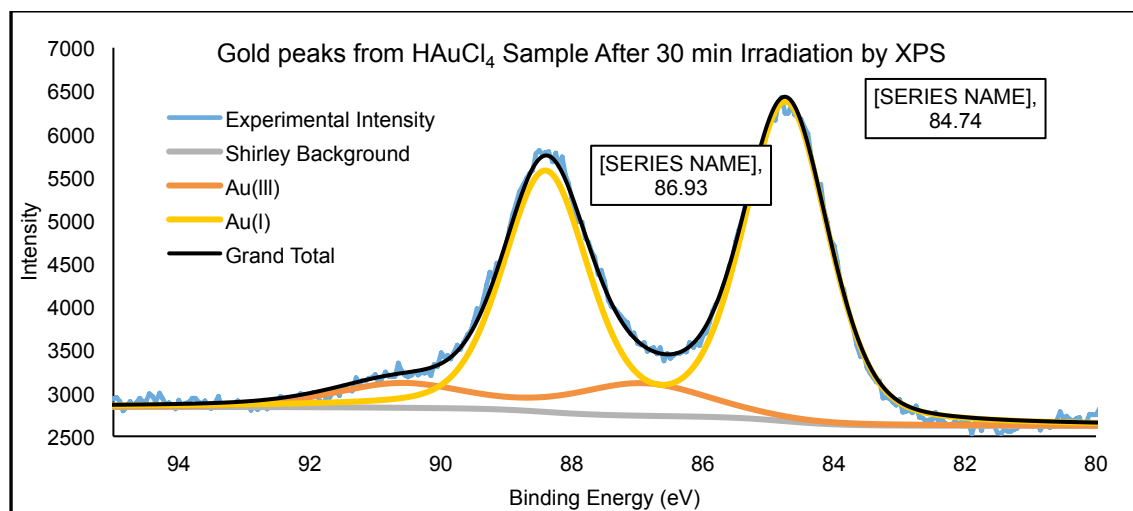

Figure 7(b): XPS Results of Chloroauric acid [HAuCl$_4$] after 30 minutes exposure to XPS

It is clear that the intensity of Au(l) increases while the Au(lll) decreases because of the photoreduction of Au(lll) during the XPS scans. The ~ 30 minutes irradiation of the sample by X-ray reduced ~ 90% of Au(lll) to Au(l). The position of the Gold peaks have been shifted to the low binding energy, 0.26 eV for Au(l) and 0.68 eV for Au(lll). We assumed this shifting was due to the charging of the sample during the measurement which was (4.75 eV) higher than expected. From this experiment, we can understand that irradiating the HAuCl$_4$ solution before the photodeposition process may increase the rate of the Au NPs deposited on TiO$_2$.

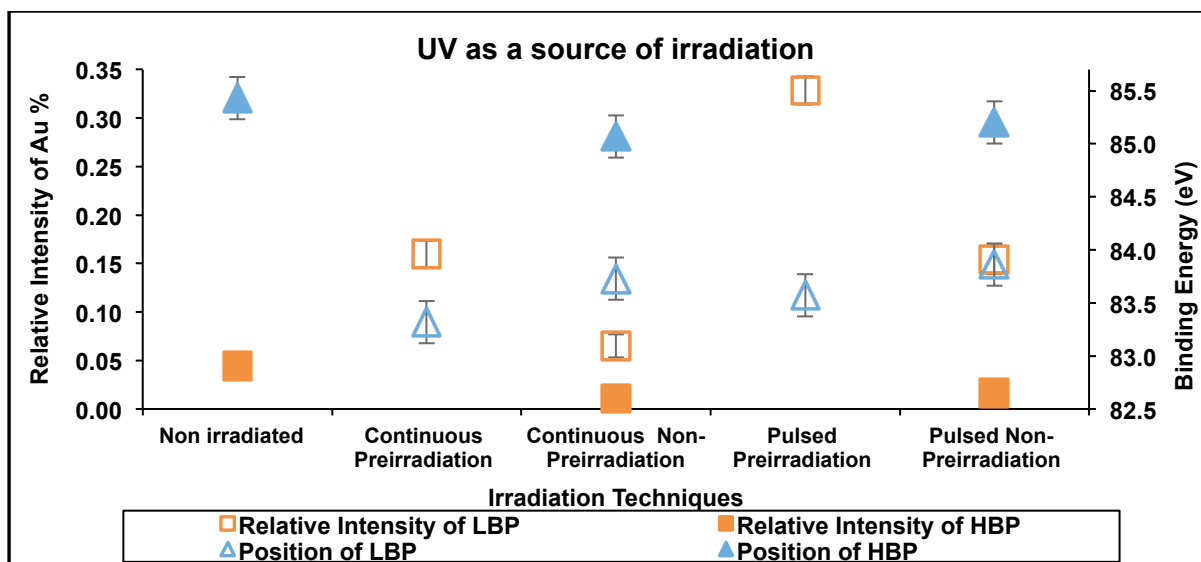## 5.2 Photodeposition of Chloroauric acid [HAuCl$_4$]

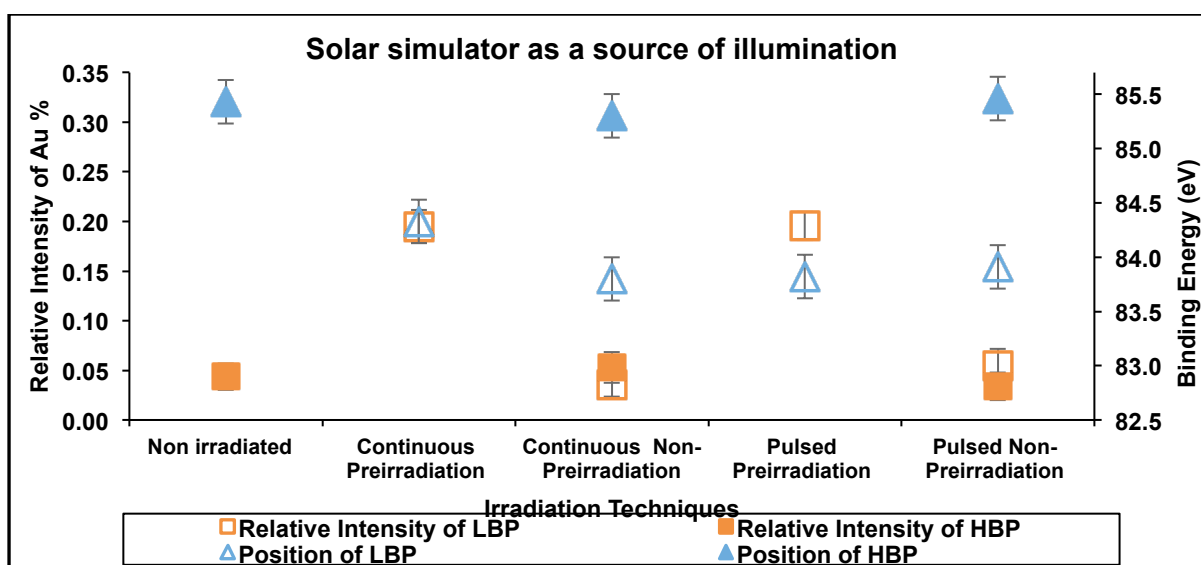**Figure 8**: XPS Results of Chloroauric acid [$HAuCl_4$] under UV source

Figure 9: XPS results of Chloroauric acid [$HAuCl_4$] under solar simulator

Here, we investigate the photodeposition of Au from $HAuCl_4$ onto TiO_2. The $HAuCl_4$ solution was preirradiated for 6 minutes before the photodeposition process. Two irradiation techniques were used to irradiate the samples (Pulsed and Continuous). The samples were illuminated by UV light and solar simulator. The relative intensity and the peaks position of Au from XPS can be seen in figure 8 and 9. The results are presented and discussed in the following sections.

Effect of Preirradiation of $HAuCl_4$ Solution

Preirradiation of the HAuCl$_4$ solution reduced Au(III) to Au(I) that could readily reduce to gold atoms Au^0 and deposited as Au NPs at the TiO$_2$ surface [18]. Due to this fact, we can see in figure 8 and 9 that the amount of Au NPs deposited onto the TiO$_2$ samples in the preirradiation solution, irradiated by UV light or solar simulator, are two to three times higher than the non-preirradiation for both continuous and pulsed techniques. Moreover, the non-preirradiation samples produce two 4f$_{7/2}$ gold peaks and the average of those peaks positions are ~ 83.80 eV and ~85.20 eV. According to the photoreduction steps of HAuCl$_4$, we assume that the first peak is Au NPs which is around the binging energy of 83.80 eV, and the second peak, according to the HAuCl$_4$ reference sample, is Au(I) which is around the binging energy of 85.20 eV. However, the second peak could be Au clusters according to the final state effect. It is expected that the association of Au^0 atoms coalesced into Au nanoclusters at the surface [37]. Nevertheless, using XPS we unable to determine if this peak is Au clusters or Au(I). Transmission electron microscopy (TEM) could be used to determine the size of the gold cluster that deposited on the surface of the TiO$_2$. Unfortunately, this could not be done because of the limited time available for this project.

Effect of Pulsing

The irradiation techniques of light exposure also seemed to play a significant role in determining the final formation of the Au-TiO$_2$ hybrid product. From figure 8 photodeposition using the UV light, it can be seen that when continuous technique is compared to the pulsed technique, the rate of the Au NPs deposited on titanium dioxide in the pulsed technique is higher than in the continuous technique for preirradiation and non-preirradiation. The likely reason for this result is that during the continuous irradiation, the gold nanoparticles grew to larger particles on the surface rather than depositing individually on the surface. We will discuss this hypothesis later using SEM images. On the other hand, during a pulsed irradiation, there is discharge of electrons between the pulses which may generates more Au NPs on the surface [20]. Also, it is possible that the sample on pulsed techniques stayed ~40 second longer on the solution comparing to the continuous technique may increase the amount of Au NPs. For illumination by solar simulator, it can be seen in figure 9 that comparing between the two irradiation techniques, there was almost equal amount of Au NPs deposited in both continuous and pulsed techniques. In the non-

preirradiation, the amount of Au NPs is a slightly higher in the pulsed technique than in the continuous technique.

Comparing between solar simulator result and UV light.

In both solar simulator and UV, Au NPs are generated at binding energy of ≈ 84.0 eV. However, the UV photodeposition process occurred much faster than in the solar simulator for pulsed technique. This is because the absorption spectrum of TiO_2 is largely found in the UV region. While the TiO_2 can absorb $\approx 2 - 3$ % of UV from solar spectrum [41]. It is important to note that the intensity of the solar simulator (147 mW/cm^2) was higher than UV lamp ($\approx$ 54 mW/cm^2). On the continuous technique they much similar. This may because on the continuous the particles grew larger rather than generating more particles on the surface.

Varying Duration of UV illumination

In this part, we used UV light for non-preirradiated solution and continuous irradiation technique with varying durations of UV exposure.
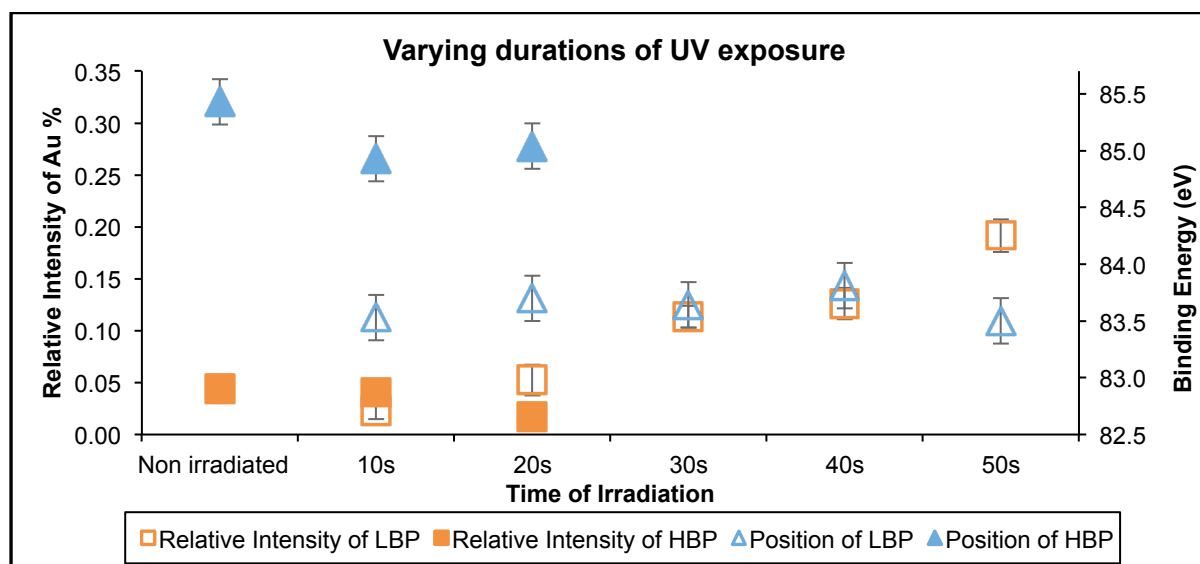

Figure 10: XPS Results of Chloroauric acid [HAuCl$_4$] under varying duration of UV illumination from 10-50 s

From figure 10, it is observed that increasing the time of exposure increases the rate of Au NPs deposition on TiO_2. The relative intensity of HBP decreases for the non-irradiated sample within the first 20 seconds, while LBP is observed to increase within the same duration and to 50 seconds. When the light absorbed by the TiO_2, it generated high-energy electrons and that reduced the Au salt at the TiO_2 interface [18]. By increasing the exposure time the Au(I) would reduce faster ,because of the effect of the electrons that generated from the TiO_2, and forms Au NPs on the surface. However, it is possible that the HBP is Au cluster and with increased time exposure, they start to aggregated to yield larger Au NPs[37]. The LBP around ≈ 83.70 eV which assigned to Au NPs position.

Varying concentrations of $HAuCl_4$ salt solution

In this part, we used UV light with non-preirradiated solution and continuous technique for a duration of 10 seconds, with varying concentrations of $HAuCl_4$.
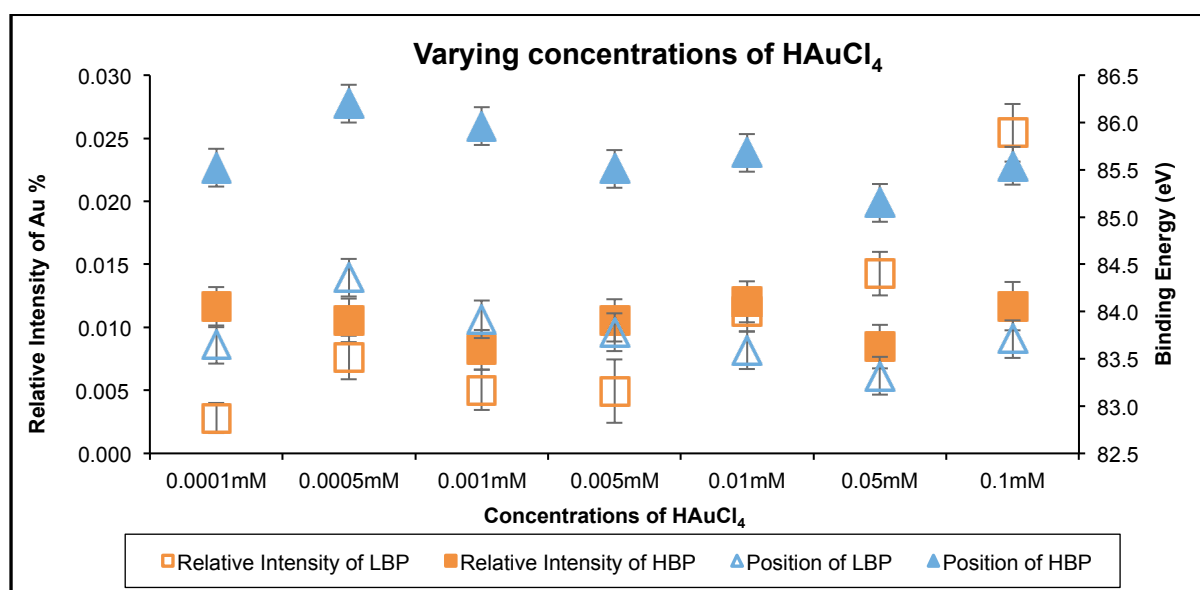

Figure 11: XPS Results of Chloroauric acid [$HAuCl_4$] under UV illumination in varying concentrations

From figure 11, it is observed that the relative intensity of HBP, which is Au(I), change slightly with varying concentrations while the LBP, which is Au NPs, increase with increasing the concentration. It is noted that there is a continuous attachment of Au(I) and stays constant while the amount of Au(I) reduced to Au^0 and forms Au NPs increases. This can

confirms that the reduction process of the $HAuCl_4$ to Au^0 similar for varying of concentrations.

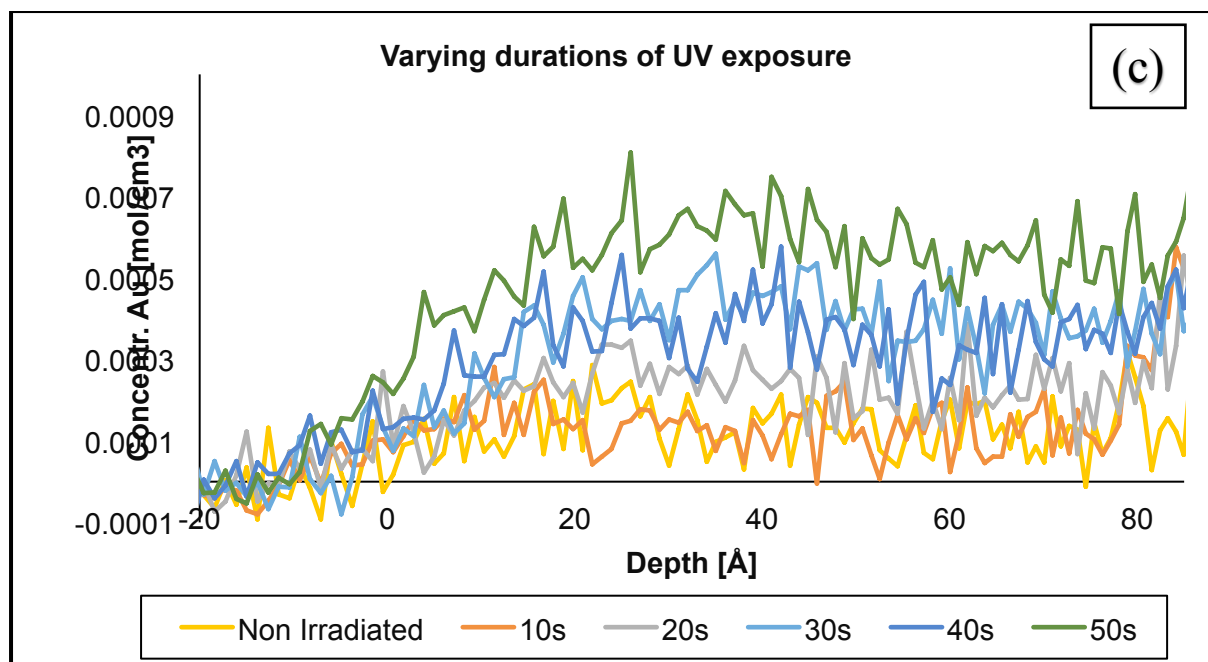**Concentration depth profiles of Au NPs from HAuCl₄**
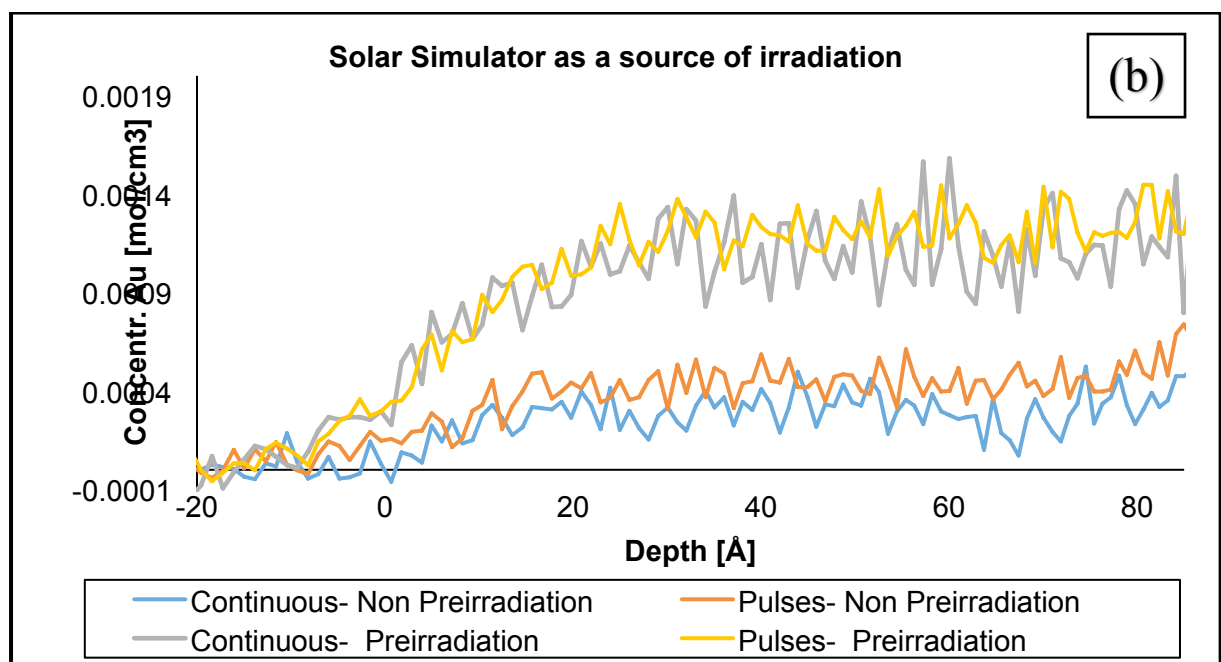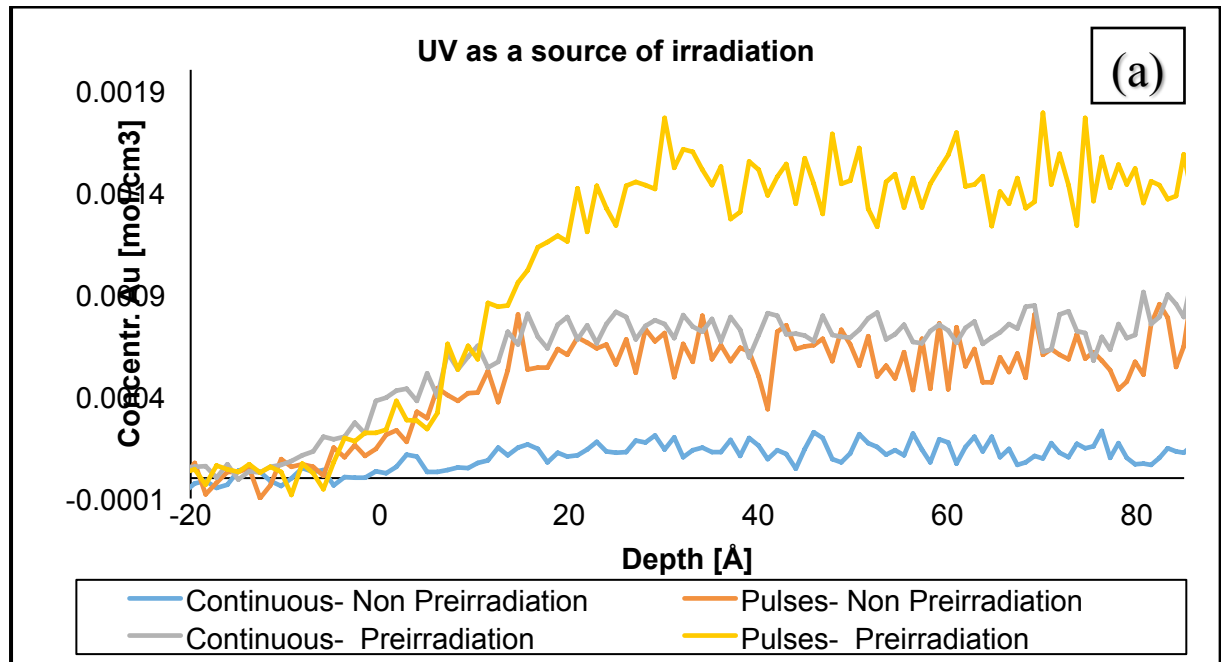
Figure 12: NICISS results showing the concentration depth profile of non-pre-irradiated and pre-irradiated Au samples illuminated the using pulsed technique and continuous technique: (a) samples irradiated using UV light (b) samples irradiated using solar simulator; and (c) samples illuminated with UV light in varying durations, with non-preirradiation solution by continuous technique.

From figure 12, we can compare the concentration depth profiles of different samples of Au NPs supported on TiO_2 with different conditions and provide information about the structure of the nanocomposite material. From figure 12 (a), (b), and (c), we can see that the concentration depth profile on same range to 85 Å which means that mostly large Au nanoparticles are formed on the surface.

The NICISS measurements in figure 12 (a) shows that more Au NPs are deposited on the surface from the $HAuCl_4$ solution in the preirradiated condition than the non-preirradiated. That because preirradiaton reduced Au(lll) to Au^0 atoms and they may forms small particles before the photodeposition process which increase the photodeposition ,prevalence, of the Au NPs on the surface. This contributes to the reason that there was a higher concentration depth profile for the preirradiated

A similar observation is also made with samples presented in figure 12 (b), where the samples were illuminated using solar simulator. It is, however, noted that the concentration of gold in samples illuminated with solar simulator is lower than in samples illuminated with

UV light (in figure 12 b). This difference in the Au deposited on the TiO$_2$ substrate is due to the fact that the absorption spectra of TiO$_2$ is in the UV region. Under direct UV, TiO$_2$ valence band electrons are excited. UV source from a solar simulator contains a smaller amount of UV, compared to a dedicated source of UV light. Only 2-3% of the solar spectrum can be absorb by TiO$_2$ [41]. This makes the photodeposition process to occur faster in the UV light than under the solar simulator, which explains the high concentration of Au on the surface of the TiO$_2$ nanomaterial illuminated using UV [18].

From the results presented in the NICISS graphs in figure 12 (a) and (b), it is observed that the photodeposition technique has a significant effect on the final products formed after continuous and pulsed irradiation. In UV light from figure 12 (a), the amount of gold deposited on the TiO$_2$ surface with the pulsed technique is one time higher than with the continuous technique. In solar simulator from figure 12 (b), it were slightly higher in pulsed technique compared to continuous. The reason is because the pulsed technique generates more Au nanoparticles on the surface while the Au nanoparticles on the continuous technique grow larger by agglomeration.

From figure 12(c), it is generally observed that as the time of exposure increases from 10 seconds to 50 second, the concentration of Au NPs increases. This is because longer times of exposure to UV illumination create a condition that allows the accumulation of electrons at the Au deposition sites. (See figure 13).
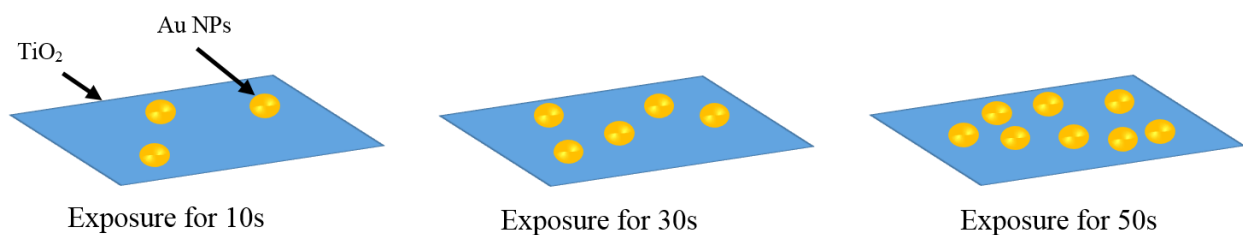

Figure 13: Increase in the concentration of gold NPs on the TiO$_2$ with increase in exposure time.

In a closed layer, it is expected that varying the amount of the substance deposited would increase the range of the concentration depth profile of Au, rather than increasing the height of the profile [32].

Valence Band of photodeposition of Chloroauric acid [HAuCl$_4$] on TiO$_2$

Using UPS we can determine the valence band of photodeposition of HAuCl$_4$ on TiO$_2$ by secondary electron cut-off at low binding energy (see figure 14).
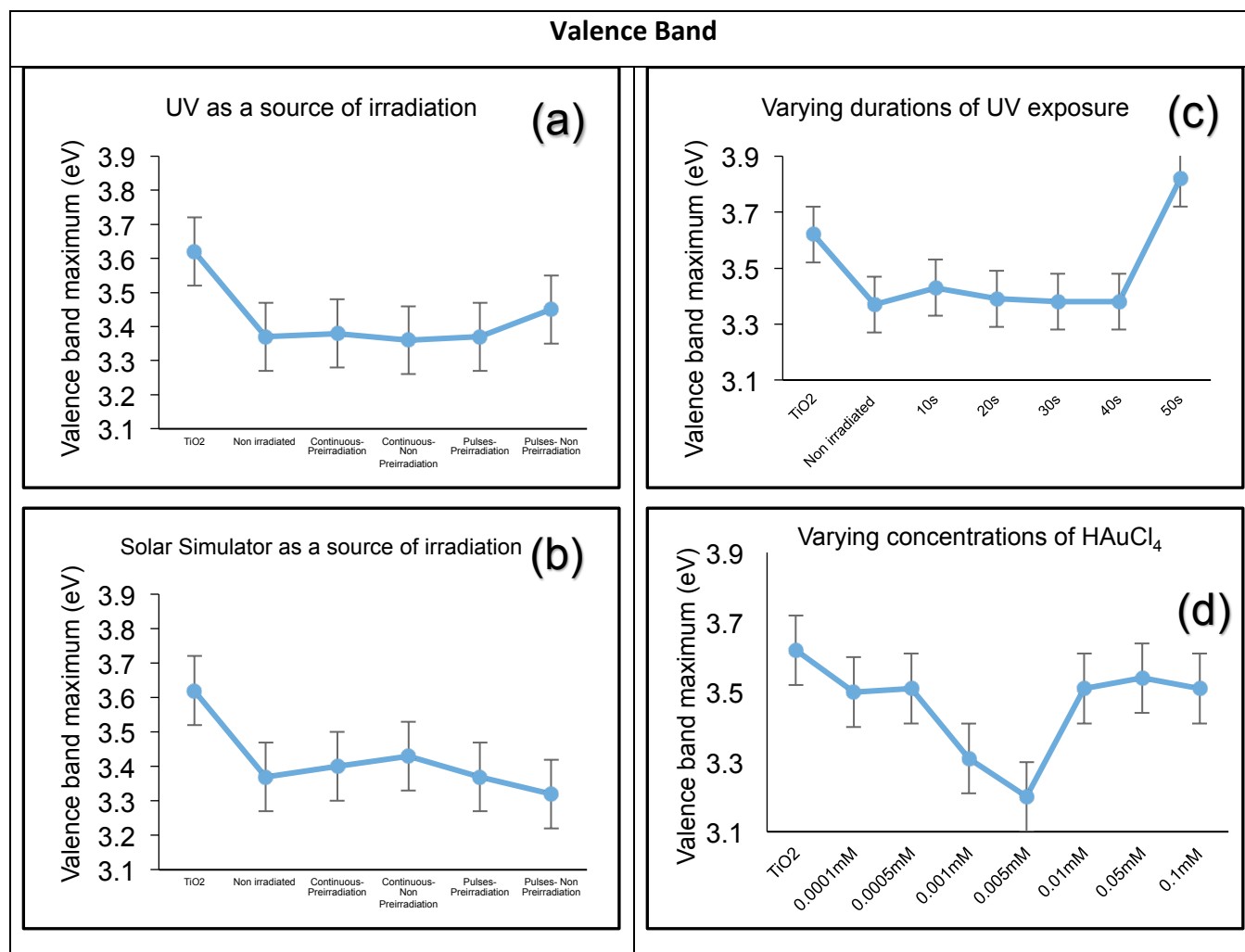

Figure 14: UPS results of TiO$_2$ sample after photodeposition of HAuCl$_4$ acid. (a): Samples exposed to UV light; (b): Samples exposed to solar simulator; (c): Samples irradiated with UV for 10s to 50s ; (d) Samples with varying concentrations of HAuCl$_4$ irradiated with UV light.

From figure 14(a), the valence band cut-off of TiO$_2$ occurs at a BE of 3.62 eV. However, this value drops after photodeposition of HAuCl$_4$ treated in different conditions. The same trend is also observed in for the non-irradiated sample where the BE is low at 3.37 eV. The valence band emission of the non-preirradiated continuous and pulses samples occurs at BE of 3.36 eV and 3.45 eV. For the pre-irradiated samples, the BE between 3.38 eV and 3.37 eV. Under UV irradiation, non-preirradiated pulsed technique appears to slightly increase the BE at which valence band emission occurs compared to the continuous technique. This is the

opposite under solar simulator, where the BE at which valence band emission occurs slightly drops with the pulsed technique. This slight change may be attributed to the fact that photodeposition of the Au NPs with different sizes onto the surface of TiO_2, changing the conditions on the surface of the material.
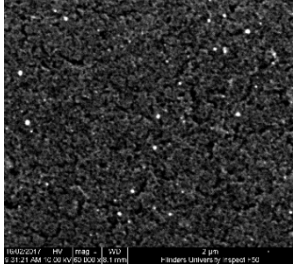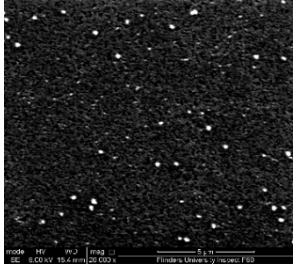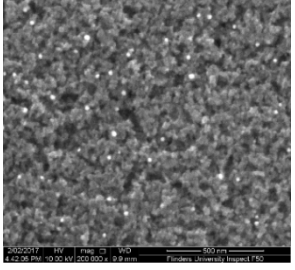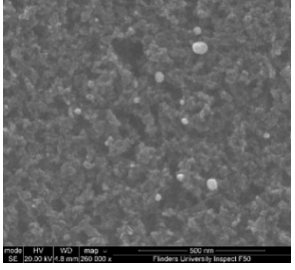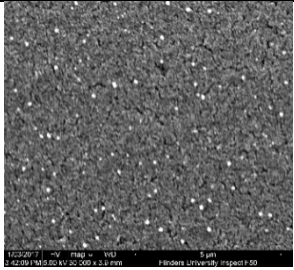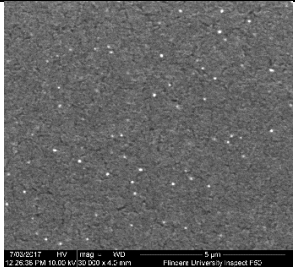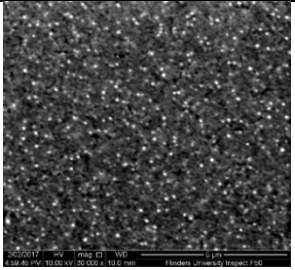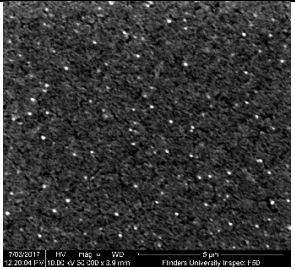
The effect of varying the duration of UV irradiation from 10s to 50s and varying concentration

Between a UV exposure of 10s and 40s, the BE at which valence band emission occurs slightly decreases from 3.43 eV to 3.38 eV (see figure 14c). As the duration of UV exposure increases to 50s, the BE of valence band increases to 3.82 eV. From figure 14(d) it is observed that as the concentration of $HAuCl_4$ increases from 0.0001 mM to 0.005 mM, the BE drops from 3.5 eV to 3.2 eV. From 0.005 mM to 0.05 mM, the valence band emission increases to a BE of 3.54 eV. We not sure what these changes on the valence band mean. To understand the photocatalytic activity of the samples we need to measure the conduction band using, for example, Inverse Photoemission Spectroscopy (IPES). That was not the aim of this particular project.

The distribution and form of the Au particles on the TiO2 surface

In this study, we used the SEM technique to study the distribution and the form of the Au nanoparticles on the surface of the TiO_2. The SEM images are presented and discussed below.

Table 1: SEM images for the investigation of prevalence of Au NPs on the surface of TiO_2 for samples illuminated by UV light and solar simulator.

Irradiation Techniques	Continuous Preirradiation	Continuous Non-Preirradiation	Pulsed Preirradiation	Pulsed Non-Preirradiation
UV				
Image				
Area by um^2	~ 21 um^2	~ 192 um^2	~ 1.9 um^2	~ 1.1 um^2
Number of particles	25	40	40	15
Particles per square micrometre	1.2	0.2	21	13.6
Solar Simulator				
Image				
Area by um^2	~ 82 um^2	~ 85 um^2	~ 85 um^2	~ 85 um^2
Number of particles	110	60	250	100
Particles per square micrometre	1.3	0.7	2.9	1.2

From Table 1, it was expected that the magnification of the SEM images would be the same so we can compare them. Unfortunately, the SEM images appear different from one another. However, for samples irradiated using solar simulator, we can observe some similarities, except for the continuous preirradiated sample in which there are

25

approximately 3 um^2 less. For samples irradiated using UV light, the SEM had several magnifications. This could not be re-addressed because of the limited time we had with this project.

From these results, we can learn two things. First, there are more particles per square micrometre on the pre-irradiated sample compared to the non- pre-irradiated sample. This is because pre-irradiation of the HAuCl$_4$ solution generates more Au NPs as we discussed before.

(a) Continuous Preirradiation

(b) Continuous Non-Preirradiation

(c) Pulsed Preirradiation
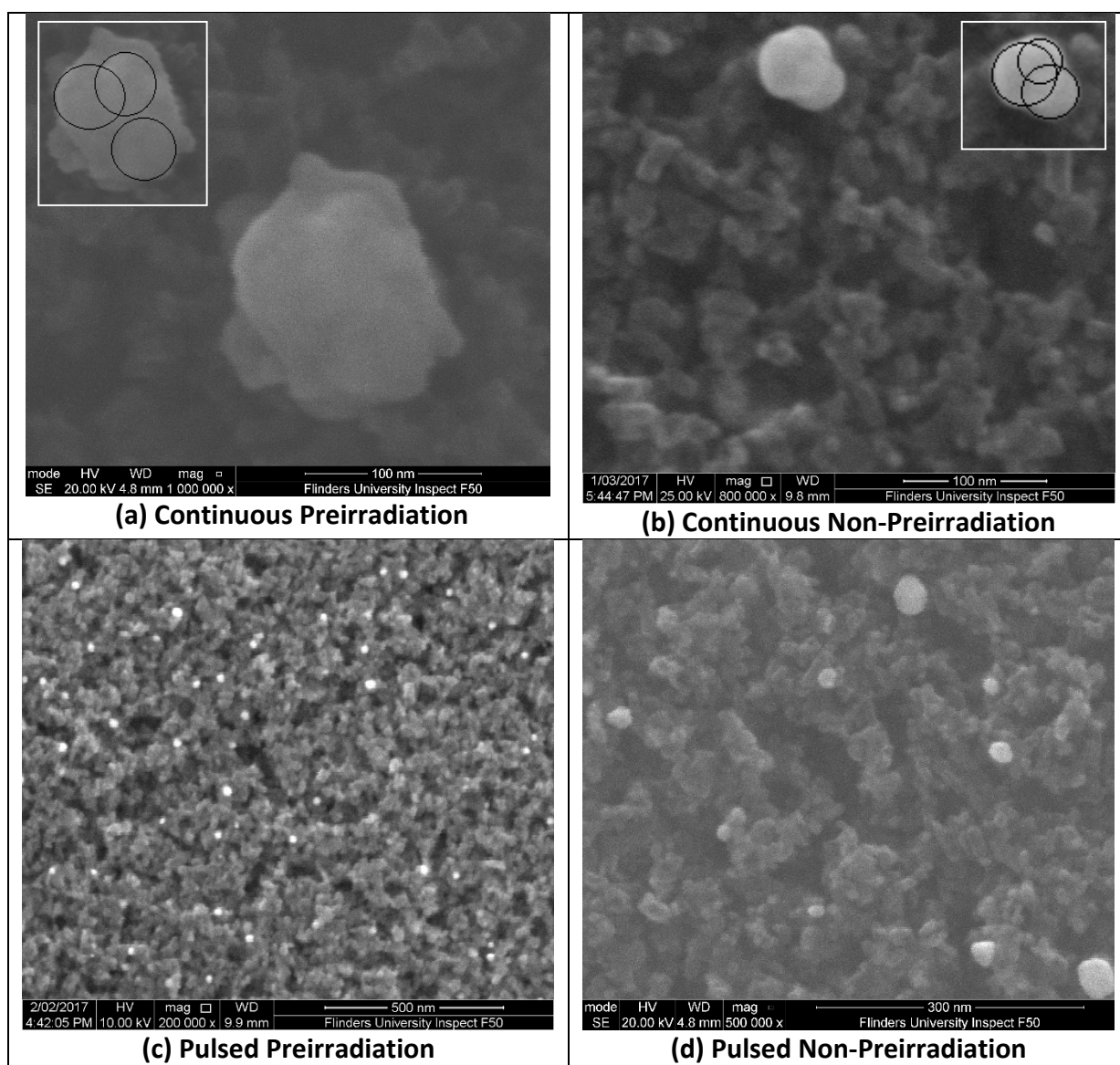
(d) Pulsed Non-Preirradiation

Figure 15: SEM images of photodeposition of Au NPs on the surface of TiO$_2$. (a):pre-irradiated sample with continuous technique, (b): Non-pre-irradiated sample with continuous technique, (c): Non-pre-irradiated sample with pulsed technique, and (d): Pre-irradiated sample with pulsed technique.

Second, it is observed that more Au NPs are deposited on the surface of the TiO_2 using the pulsed technique, while using the continuous technique produces approximately about half of the amount of Au NPs. This because by using the continuous technique, the Au particles grew larger due to the effect of the excitation of the electron in the TiO_2 which reduced the Au on the surface and grew larger [18]. While the 30 seconds gap on pulsed illumination help to generated more (small-size) particles on the surface of TiO_2. Furthermore, it can be observed in figure 15(a) that Au NPs were agglomerated into larger Au NPs by irradiating the sample in pre-irradiated solution using continuous technique. In the image in figure 15(b), it show that there were two or three Au NPs gathered together. There is less agglomeration exhibited, which is attributed to the fact that Au(lll) needs to reduce to Au(l) then Au^0 to form Au NPs during the photodeposition. However, the pulsed technique generated smaller particles for both pre-irradiated and non-pre-irradiated (see figure 15c and 15d).

Conclusions

We have successfully used XPS, NICISS, UPS and SEM techniques to study the photodeposition of $HAuCl_4$ on TiO_2 nanoparticles. Preirradiation of $HAuCl_4$ solution can increase the rate and amount of Au NPs photodeposited onto the surface of TiO_2. This is due to activation of the Au salt prior to photodeposition. It was observed that photodeposition occurred higher in samples illuminated with UV light than in samples illuminated with solar simulator for pulsed. Using pulsed irradiation technique resulted to more Au NPs being deposited on the surface of TiO_2, compared to continuous technique. Pulsed technique favours the formation of small Au NPs, while continuous technique favours the formation of large Au NPs due to agglomeration of the Au NPs during the continuous technique. Increasing the time of exposure to UV light and the concentration of $HAuCl_4$ also increases the amount of Au NPs deposited on the surface of TiO_2. These results are supported by NICISS and SEM. The NICISS results shows that the Au NPs forms large on the surface of the TiO_2.

5.3   Photodeposition of Au clusters $[Au_9\,(PPh_3)_8)]\,(NO_3)_3$

For this type of gold, we used the UV light only with non-preirradiation and continuous illumination technique.

It is important to note here that for XPS results, the position of the Au peaks related to the size of the cluster whether they form larger groups "agglomerated" of Au_9 clusters or are deposited individually on the surface [23].

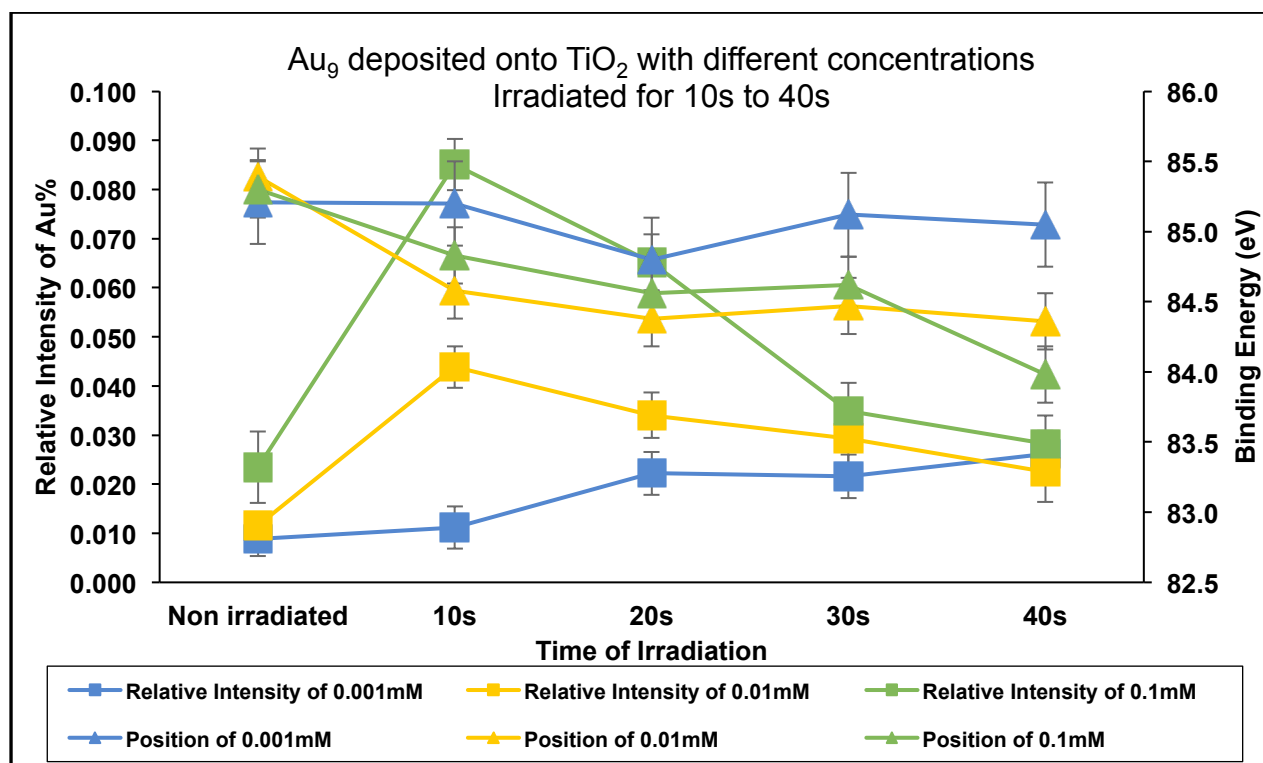**Different concentrations of Au_9 with different irradiation time**

Figure 16: XPS for different concentrations of Au_9 under different durations of illumination

From figure 16, it can be see that the relative intensity of Au cluster increase for all varying concentrations after 10s exposure to UV light. However, it can be observed that at a concentration of 0.1mM and 0.01mM, the relative intensity of Au_9 decreases as the duration of irradiation increases. Moreover, the binding energy also shifts from 85 eV to 84 eV for samples irradiated in concentration of 0.1mM and from 85 eV to 84.5 eV for concentration of 0.01mM. That means the clusters begin to grow to form larger particles (agglomeration) as irradiation time increases for both concentration 0.1mM and 0.01mM. At a concentration level of 0.001mM, the relative intensity of Au_9 increases as the duration of irradiation increases. The binding energy remains relatively stable at about 85 eV and that means the Au form isolated a cluster on the surface [1].

Annealing

To investigate the size of the clusters, annealing of the photodeposited of Au_9 on TiO_2 samples was carried out by heating the samples at 200°C under high vacuum (10^{-4} mbar) for 10 minutes to remove the phosphine (PPh_3) ligands for activating the deposited clusters as catalytic sites [21]. The results before and after heating for different concentrations (0.1mM, 0.01mM, and 0.001mM) are presented in figures 18 to 20. After annealing the samples, the PPh3 ligands which protect the Au_9 clusters are lost and two things can occur: either the Au_9 cluster cores maintain their identity; or the cluster cores merge to form larger particles (see figure 21) [16]. The binding energy as found by XPS for gold cluster is dependent on the final state effects which relate to the size of the Au cluster [22]. Therefore, the binding energy will decrease when the clusters agglomerated.

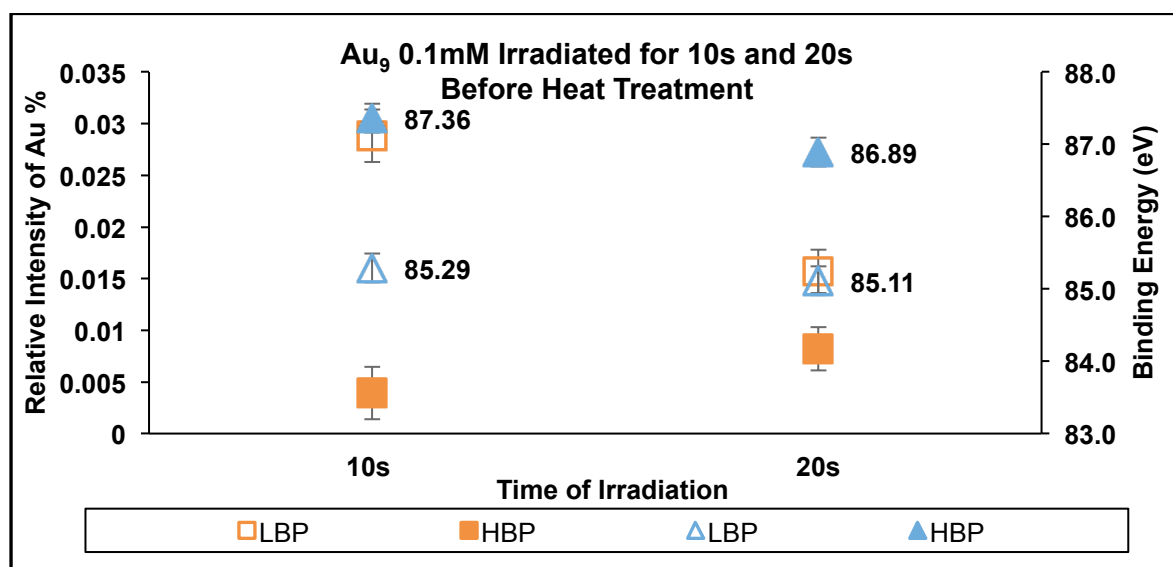**Before and after heat treatment of 0.1mM Au_9 irradiated for 10s and 20s**

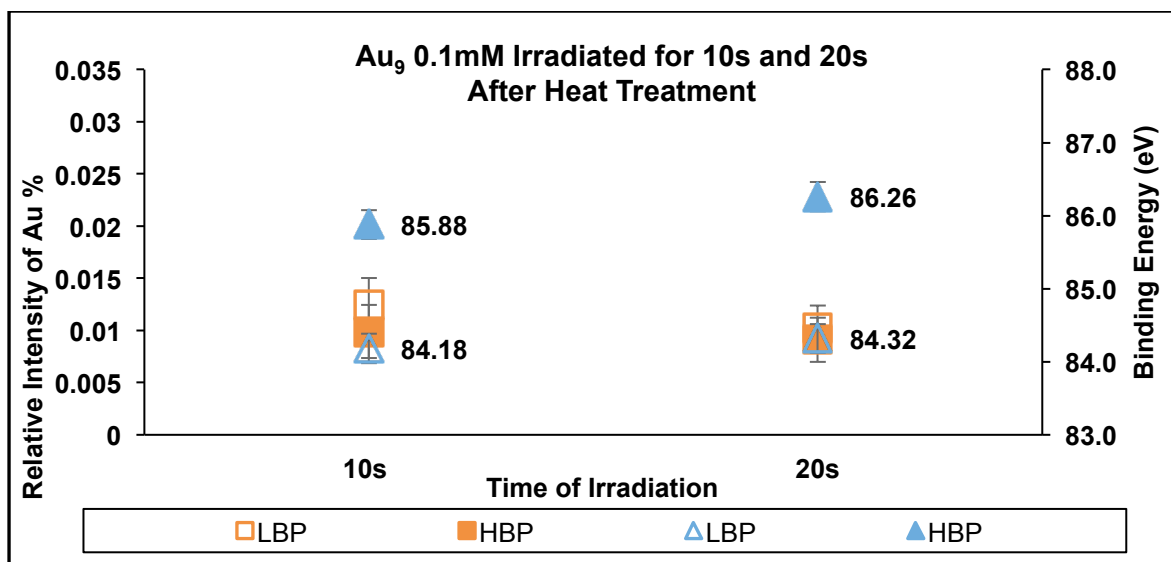*Figure: 18(a)*: 0.1mM Au_9 before heat treatment

Figure: 18(b): 0.1mM Au_9 after heat treatment

Before heating, the LBP position is above 85 eV for both samples (irradiated for 10s or 20s), and after heating, the LBP position decreases to be around 84 eV. The LBP relative intensity for samples irradiated for 10 and 20 seconds were high before heat treatment and dropped after the treatment(see figure 18(a) and (b)). Also, heat treatment results see a decrease in the HBP position from ~87.40 eV to ~85.90 eV for 10s sample and from ~86.90 eV to ~86.30 eV.

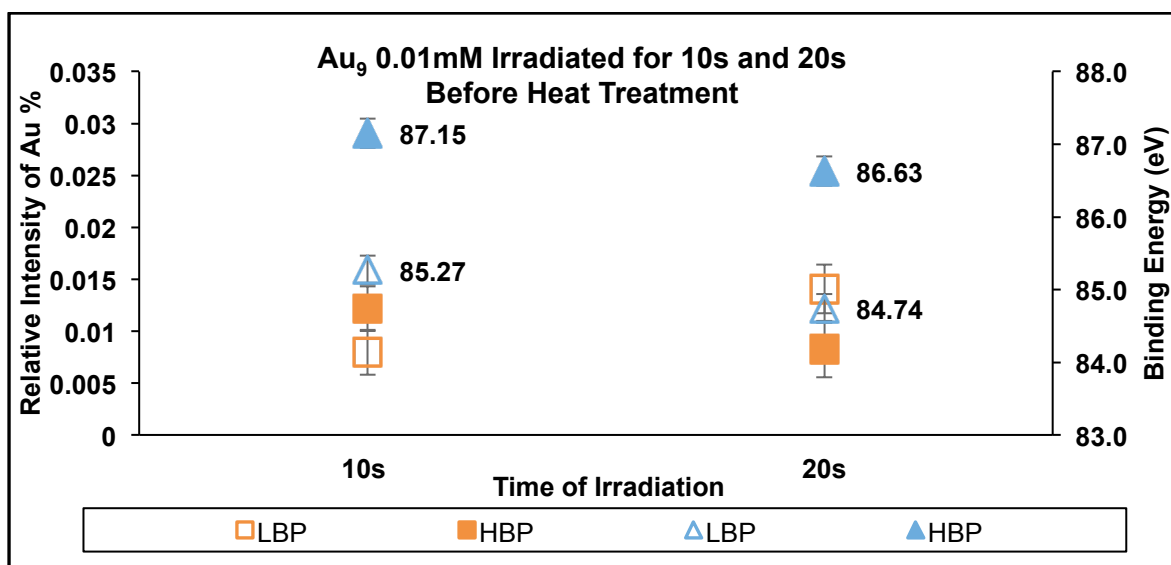**Before and after heat treatment of 0.01mM Au_9 irradiated for 10s and 20s**

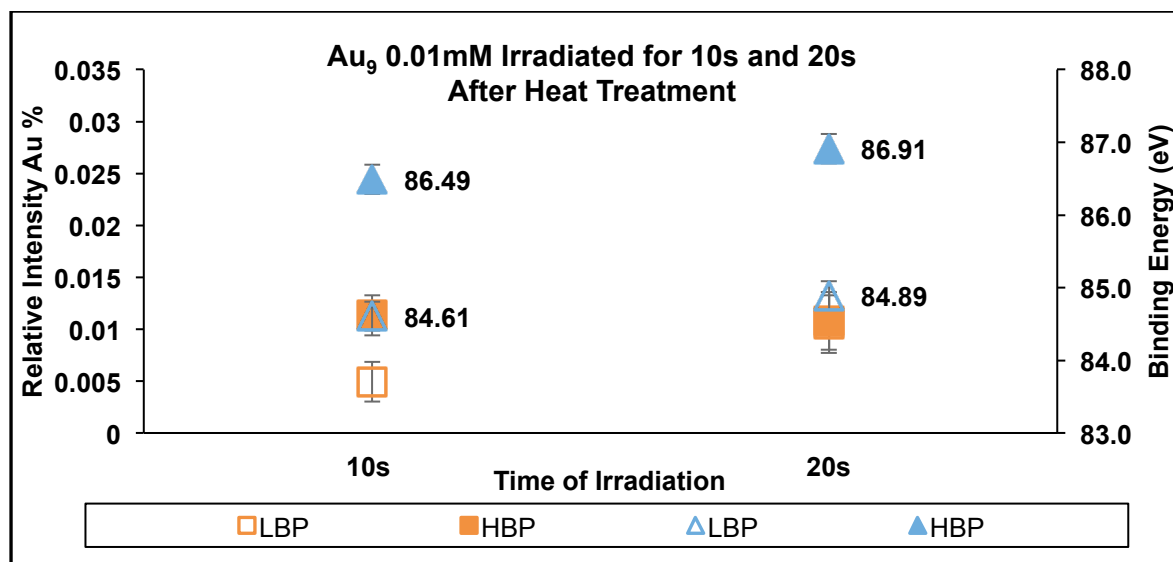**Figure 19(a)**: 0.01mM Au_9 before heat treatment

Figure 19(b): 0.01mM Au$_9$ after heat treatment

Before heating, Au clusters are obtained at binding energy of 85.27 eV within 10 seconds irradiation. After heating from the LBP, Au clusters partially agglomerate at binding energy of 84.61eV. That was not the case for 20s, before heating the LBP at 84.74 eV and increasing to 84.89 eV while the relative intensity decreases after heating. The HBP position decrease after heating from ~87.15 eV to ~86.49 eV for 10s sample and from ~86.63 eV to ~86.91 eV.

Before and after heat treatment of 0.001mM Au$_9$ irradiated for 10s and 20s
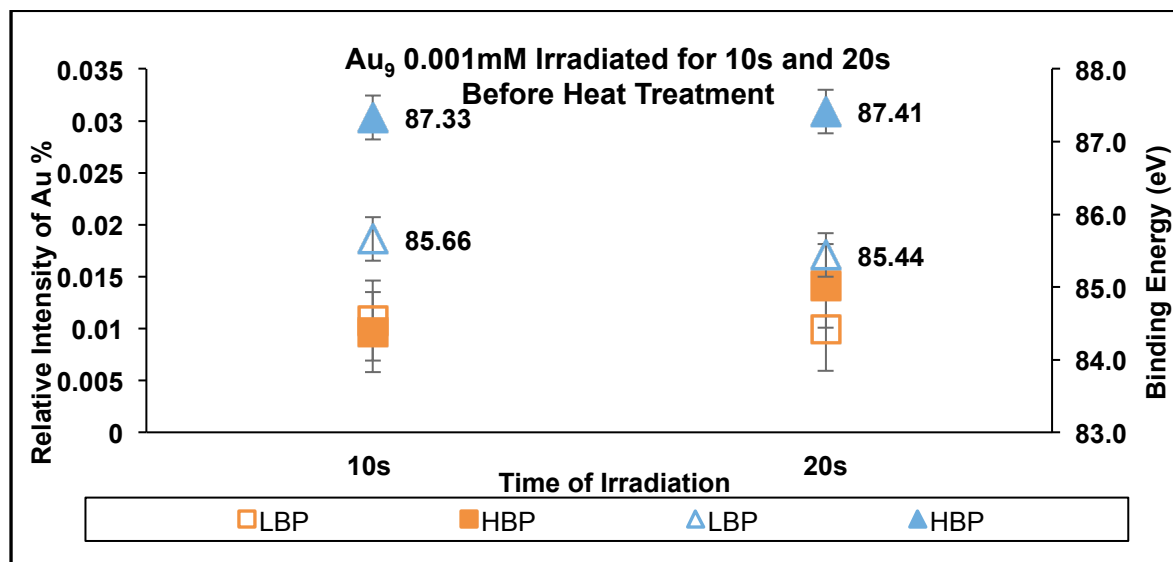

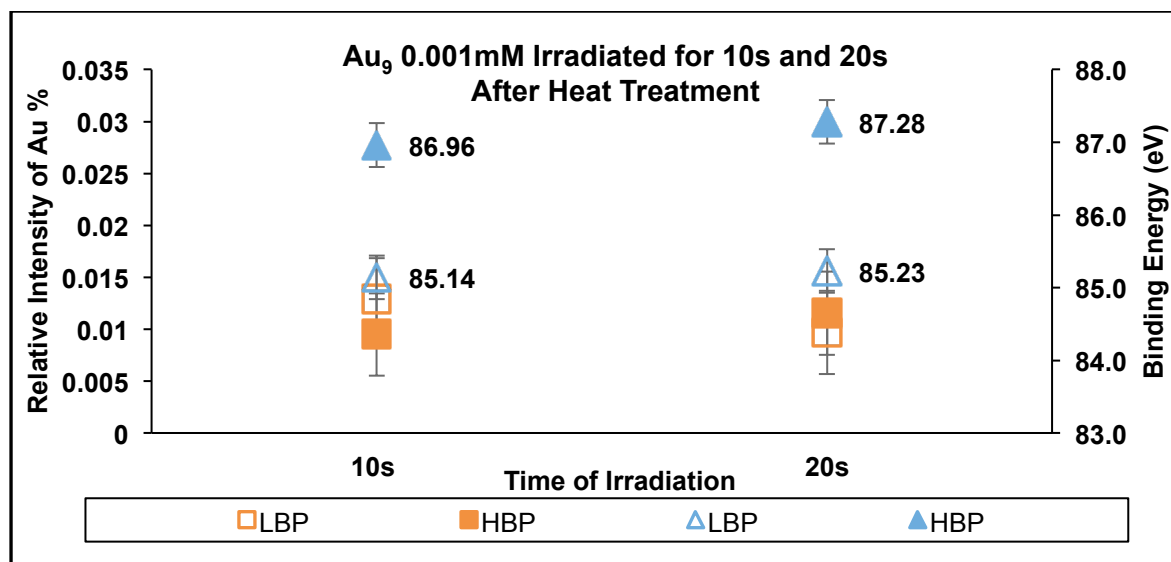**Figure 20(a)**: 0.001mM Au$_9$ before heat treatment

Figure 20(b): 0.001mM Au$_9$ after heat treatment

Before heating, the Au clusters are obtained at the LBP of 85.66 eV and 85.44 eV for 10 and 20 seconds irradiation. After heat treatment, the ligands were removed and the LBP decreases to 85.14eV and 85.23 eV which is relative to Au clusters position. The HBP position decrease after heating from ~87.33 eV to ~86.96 eV for 10s sample and from ~87.41 eV to ~87.28 eV.

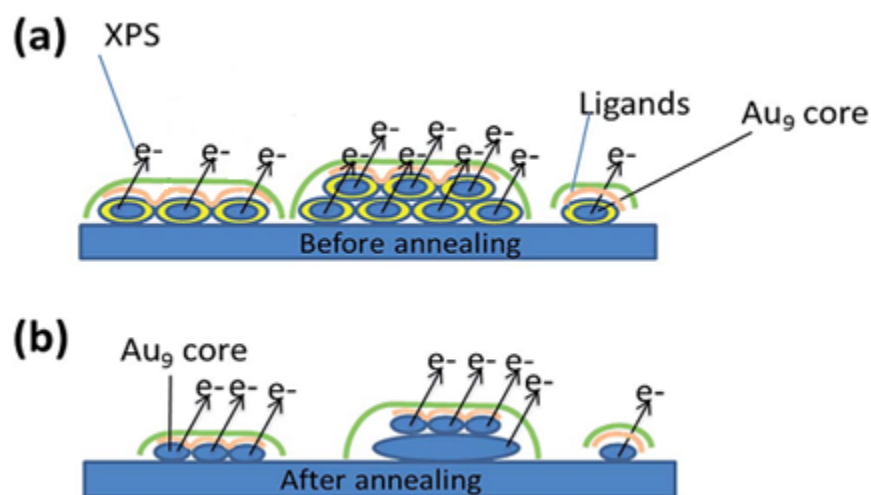**Figure 21**: A schematic diagram of Au nanoclusters deposited on TiO$_2$ **(a)** before and **(b)** after annealing (*Source*: [21]).

It is clear that before heat treatment for varying concentration the LBPs at ~ 85 eV which are intact clusters. The HBP before and after heat treatment around ~86 - 87 eV. The Au cluster peak at ~ 85 eV and below that is agglomerated cluster attributed to final state effects. The

peak at 86 eV and above we do not know what this peak means so the attribute of this peak could not be made [1].

For concentration of 0.1mM after heat treatment, the downward shift in the low binding energy peaks is attributed to the fact that Au becomes agglomerated after heating to form larger aggregates. Agglomeration of Au clusters affects its signal intensity, and thus, its peak position [23].

For concentration of 0.01mM after heat treatment, from the LBP the Au clusters were partially agglomerated for sample irradiated for 10 seconds while the sample irradiated for 20 seconds were partially agglomerated before and after heating by the effect of increasing the irradiation time. Figure 17 displays the agglomeration of the clusters with increase the irradiation time. However, the agglomeration is less for Au_9 concentration of 0.01 mM compared to the 0.1mM.

For concentration of 0.001mM after heat treatment, a peak at the low binding energy shows that position at ~ 85 eV which are non-agglomerated clusters.

The agglomeration of the Au clusters also plays a role on the intensity of the signal obtained. Because there is limited electron mean free path, electrons that originate from larger clusters tend to be attenuated more, compared to those emitted from smaller size clusters [23]. That can be seen in figure 21 that before annealing more electron ejected from the cluster than after annealing. That attributes to why the intensity drops after heat treatment for Au_9 0.1mM and 0.01mM.

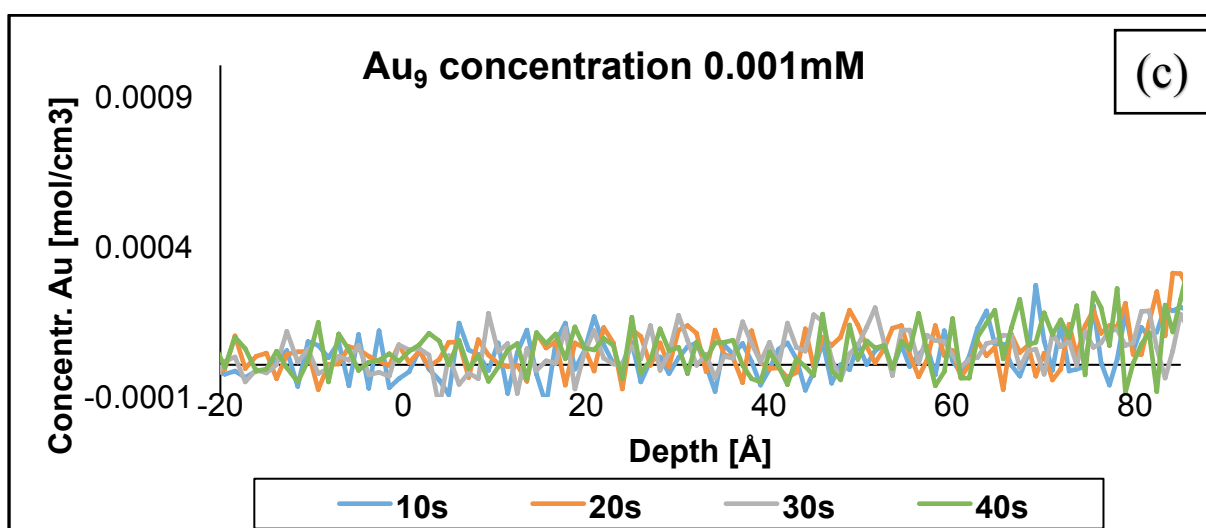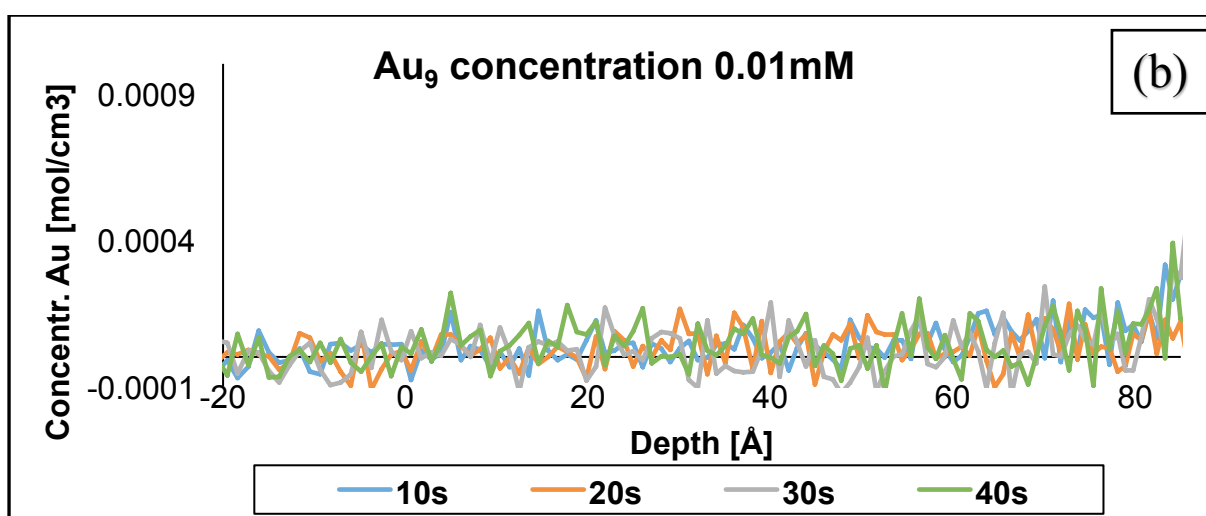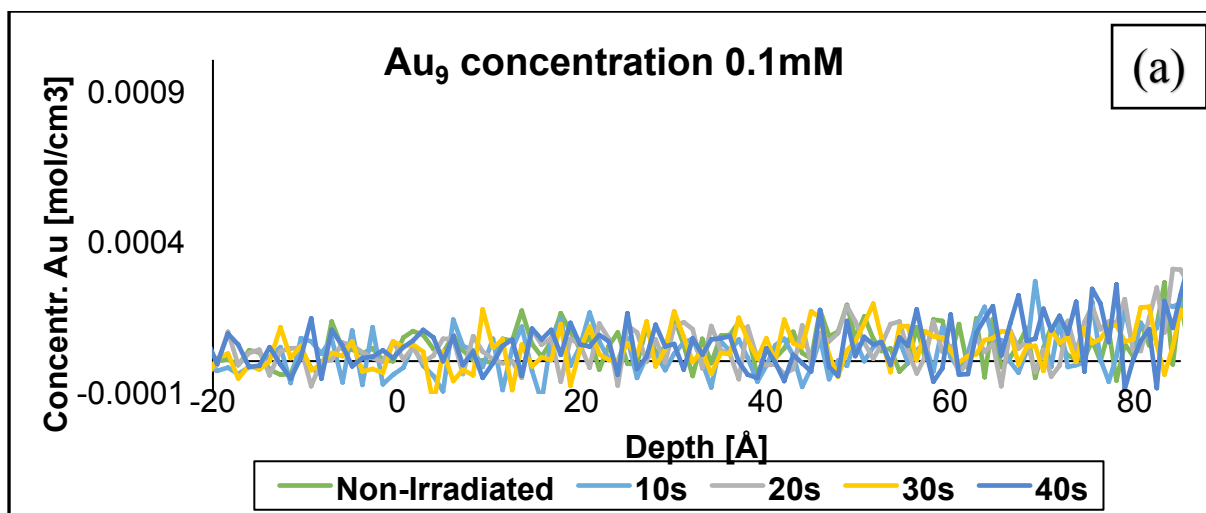**Concentration depth profiles of Gold clusters**

Figure 22: NICISS results showing the concentration depth profile of samples illuminated with UV for 10 to 40 seconds: (a) sample concentration = 0.1 mM (b) sample concentration = 0.01 mM; and (c) sample concentration = 0.001 Mm.

From the NICISS results for the Au_9 samples shown in figure 22 (a, b, c) above, nothing clear can be observed from the graphs as the profiles appear like one single profile. The slope of the onset of all the Au concentration depth profile curves appear to be almost the same for all the depths, irrespective of the duration of illumination. From the XPS results, the relative intensity of the Au_9 for sample irradiated for 10 seconds in concentration of 0.1mM was 0.1 % however no signal can be observed of the same sample from NICISS (See figure 22 (a)). Comparing this to $HAuCl_4$ sample, for example non-preirradiation solution and pulsed technique irradiated by UV lamp, the relative intensity of the Au was 0.1 % and from NICISS, the concentration depth profile of the Au was ~0.0005 mol/cm^3. That means based on the XPS intensity the concentration depth profile of the Au_9 should be around ~0.0005 mol/cm^3, but as we can see from the NICISS graphs in figure 22, nothing can be observed. This may due to the fact that it is not possible to see the gold clusters (even if they agglomerated) using the NICISS technique directly as it requires lateral resolution.

Valence band of Au_9 Clusters with varying the concentrations and durations of irradiation

The UPS results of the Au_9 clusters at different concentrations and durations of irradiation are shown in figure 23 below. It is observed that the secondary electron cut-off, decreases from the non-irradiated sample to samples irradiated for a duration of 40s, and increases with reducing concentration. The BE at the valence band remains relatively stable as 3.36 eV at irradiation time above 10 seconds except the lower concentration.
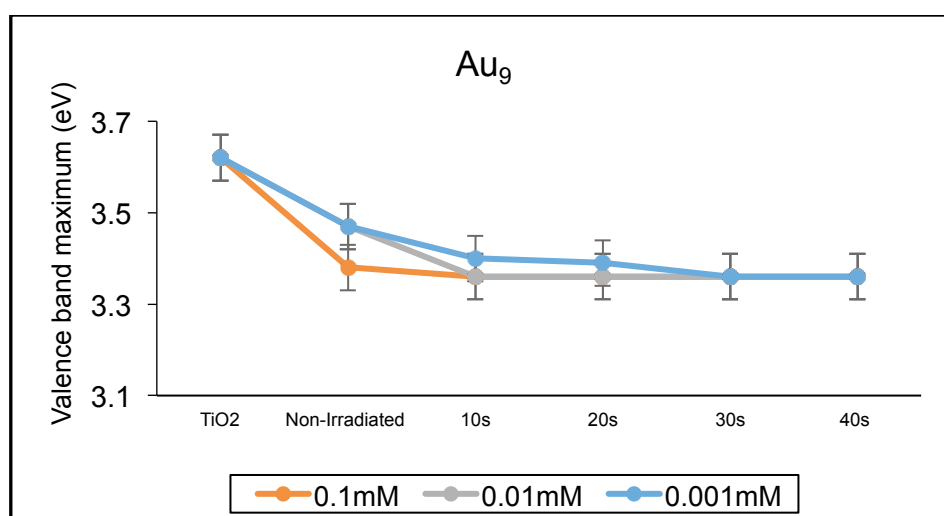

Figure 23: UPS results of Au_9 clusters

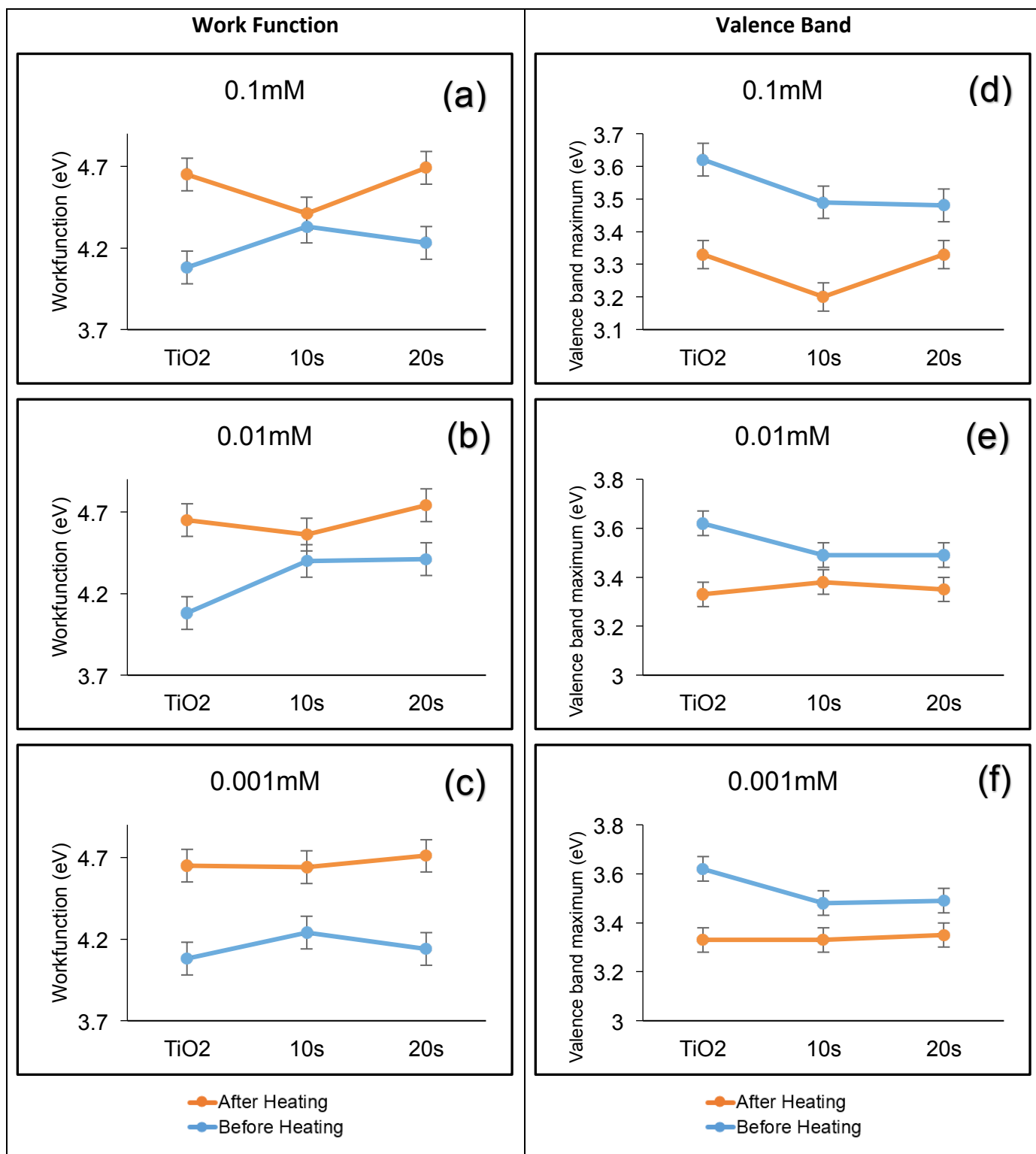**Work function and valence band of Au$_9$ before and after heating for different concentrations**

Figure 24: UPS results showing the work function and valence band of Au$_9$ before and after heating for different concentrations.

Work function of Au$_9$

In figure 24 (a, b, and c), the results of the work function of Au$_9$ before and after heat treatment with varying concentrations have been shown. For TiO2 sample, the work function before heating was 4.08 eV and after heating increase to 4.65 eV change about 0.57 eV. For concentration 0.1mM, 0.01mM and 0.001mM, the work function appears to increase 0.46 eV, 0.33 eV and 0.57 eV for sample irradiated for 20 seconds after heat treatment.

Valence Band of Au$_9$

For the valence band (see figure 24 d, e, and f), the BE at which valence band cut-off is observed to decrease after heat treatment for TiO2 from 3.62 eV to 3.33 eV. For concentration 0.1mM, 0.01mM and 0.001mM, the valence band cut-off decrease about 0.29 eV, 0.11eV, and 0.19 eV after heating for those samples exposure to UV light for 10 seconds. The highest decrease was for concentration of 0.1mM which may the present of the Au clusters on the surface is responsible for that. For samples irradiated for 20 seconds, the valence band cut-off decrease for 0.15 eV, 0.14 eV, and 0.14 eV after heat treatment.

Conclusion

We have successfully used XPS, NICISS, and UPS techniques to study the photodeposition of Au$_9$ on TiO$_2$ nanoparticles. The XPS results show that for Au$_9$ with 0.1mM and 0.01mM concentrations, the Au$_9$ agglomerated with increase the exposure time. Nevertheless, For Au$_9$ with 0.001mM concentration, the Au$_9$ non-agglomerated with increase the exposure time. Heat treatment of the Au$_9$ clusters causes particle agglomeration for 0.1mM and 0.01mM, which is attributed to the fact that the PPh3 ligands which protect the Au$_9$ clusters are lost after the annealing process. For 0.001mM, after heat treatment it produces non-agglomerated clusters. From NICISS results, we could not determine the concentration depth profiles of Au clusters. UPS had been used to locate the change of the valence band and the work function before and after heat treatment.

References

1. Anderson, D. P. et al., 2013. Chemically-synthesised, atomically-precise gold clusters deposited and activated on titania. *Phys. Chem. Chem*. Phys, Volume 15, pp. 3917--3929.
2. Bloh, J. Z., Dillert, R. & Bahnemann, D. W., 2012. Designing Optimal Metal-Doped Photocatalysts: Correlation between Photocatalytic Activity, Doping Ratio, and Particle Size. *The Journal of Physical Chemistry*, Volume 116, p. 25558–25562.
3. Britt Hvolbæk1, T. V. W. J. B. S. C., Falsig, H., Christensen, C. H. & Nørskov1, J. K., 2007. Catalytic Activity of Au Nanoparticles. *Nanotoday*, 2(4), pp. 14-19.
4. Chong, M. N., Jin, B., Chow, C. W. & Saint, C., 2010. Recent developments in photocatalytic water treatment technology: A review. *Water research*, Volume 44, pp. 2 9 9 7 - 3 0 2 7.
5. Chusuei, C. C. et al., 2001. A Nanoscale Model Catalyst Preparation: Solution Deposition of Phosphine-Stabilized Gold Clusters onto a Planar TiO2(110) Support. *Langmuir*, Volume 17, pp. 4113-4117.
6. Fujishima, A., Rao, T. N. & Tryk, D. A., 2000. Titanium dioxide photocatalysis. *Journal of Photochemistry and Photobiology C: Photochemistry Reviews*, Volume 1, p. 1–21.
7. Heiz, U. & Landman, U., 2008. *Nanocatalysis*. 1st ed. New York: Springer.
8. Lim, D.-C., Hwang, C.-C., Gantefo, G. & Kim, Y. D., 2010. Model catalysts of supported Au nanoparticles and mass-selected clusters. *Physical Chemistry Chemical Physics*, Volume 12, p. 15172–15180.
9. Linsebigler, A. L., Lu, G. & John T. Yates, J., 1995. Photocatalysis on TiOn Surfaces: Principles, Mechanisms, and Selected Results. *Chemical Review,* Volume 95, pp. 735-758.
10. Meyer, R., Lemire, C. & Shaikhutdinov, S. K., 2004. Surface Chemistry of Catalysis by Gold. *Gold Bulletin*, pp. 72-116.
11. Ohyama, J. et al., 2011. Modification of Metal Nanoparticles with TiO2 and Metal-Support Interaction in Photodeposition. *ACS Catalysis*, Volume 1, p. 187–192.
12. Primo, A., Corma, A. & a, H. G., 2011. Titania supported gold nanoparticles as photocatalyst. *Physical Chemistry Chemical Physics*, Volume 13, p. 886–910.
13. Tada, H., Fujishimaa, M. & Kobayashi, H., 2011. Photodeposition of metal sulfide quantum dots on titanium(IV) dioxide and the applications to solar energy conversion. *Chemical Society Review*, Volume 40, p. 4232–4243.
14. Wenderich, K. & Mul, G., 2016. Methods, Mechanism, and Applications of Photodeposition in Photocatalysis: A Review. *Chemical Reviews*, p. 14587–14619.
15. Zhao, J. & Yang, X., 2003. Photocatalytic oxidation for indoor air puri&cation: a literature review. Building and Environment, Volume 38, p. 645–654.
16. Anderson, D. P. et al., 2013. Chemically synthesised atomically precise gold clusters deposited and activated on titania. Part II. *Phys. Chem. Chem. Phys.*, Volume 15, pp. 14806--14813.
17. Chong, S. & Yang, T. C.-K., 2017. Illumination wavelength and time dependent nano gold photo-deposition and CO oxidation. *Results in Physics*, Volume 7, p. 1167–1174.

18. Fernando, J. F. S. et al., 2016. Controlling Au Photodeposition on Large ZnO Nanoparticles. *Applied Materials and Interfaces*, Volume 8, p. 14271–14283.

19. Nguyen, B. H. & Nguyen, V. H., 2015. Recent advances in research on plasmonic enhancement of photocatalysis. *Advances in Natural Sciences: Nanoscience and Nanotechnology*, Volume 6, pp. 1-17.

20. Primo, A., Cormaa, A. & Garcíaa, H., 2011. Titania supported gold nanoparticles as photocatalyst. *Phys. Chem. Chem. Phys.,* Volume 13, pp. 886-910.

21. Qahtani, H. S. A. et al., 2016. Grouping and aggregation of ligand protected Au9 clusters on TiO2 nanosheets. *RSC Adv*, Volume 6, p. 110765–110774.

22. Qahtani, H. S. A. et al., 2017. Aggregation Behavior of Ligand-Protected Au9 Clusters on Sputtered Atomic Layer Deposition TiO2. *Journal of Physical Chemistry*, pp. A-I.

23. Ruzicka, J.-Y.et al., 2015. Toward Control of Gold Cluster Aggregation on TiO2 via Surface Treatments. *Journal of Physical Chemistry*, Volume 119, p. 24465–24474.

24. Chambers, Benjamin A., et al. "The direct measurement of the electronic density of states of graphene using metastable induced electron spectroscopy." *2D Materials* (2017): 1-11.

25. Hiifner, Stefan. *Photoelectron Spectroscopy: Principles and Applications*. New York : Springer, 2003. Book.

26. Moulder, John F., et al. *Handbook of X-ray Photoelectron Spectroscopy*. United States of America: Physical Electronics, Inc., 1995.

27. Reimer, Ludwig. *Scanning Electron Microscopy: Physics of Image Formation and Microanalysis*. New York: Springer, 1998.

28. Ridings, Christiaan and Gunther G. Andersson. "Deconvolution of NICISS profiles involving elements of similar masses." *Nuclear Instruments and Methods in Physics Research B* (2014): 63–66.

29. Ridings, Christiaan, Vera Lockett and Gunther Andersson. "Comparing the charge distribution along the surface normal in the [C6mim]+ ionic liquid with different anions." *Colloids and Surfaces A: Physicochemical and Engineering Aspects* 413 (2012): 149–153.

30. Smart, Roger, et al. "X-ray Photoelectron Spectroscopy." 2017. 8 May 2017. <http://mmrc.caltech.edu/SS_XPS/XPS_PPT/XPS_Slides.pdf>.

31. Andersson, G. & Ridings, C., 2014. Ion Scattering Studies of Molecular Structure at Liquid Surfaces with Applications in Industrial and Biological Systems. *Chemical Reviews,* Volume 114, p. 8361–8387.

32. Lee W. Hoffman, G. G. A., Sharma, A., Clarke, S. R. & Voelcker, N. H., 2011. New Insights into the Structure of PAMAM Dendrimer/Gold Nanoparticle Nanocomposites. *Langmuir*, Volume 27, p. 6759–6767.

33. Ridings, C., Warrb, G. G. & Andersson, G. G., 2012. Composition of the outermost layer and concentration depth profiles of ammonium nitrate ionic liquid surfaces. *Phys. Chem. Chem. Phys.*, Volume 14, p. 16088–16095.

34. Borodin, ndriy and Michael Reichling. "Characterizing TiO2(110) surface states by their work function." *Phys. Chem. Chem. Phys.* (2011): 15442–15447.

35. Halder, Avik and Vitaly V. Kresin. Nanocluster ionization energies and work function of aluminum, and their temperature dependence. Los Angeles: Department of Physics and Astronomy, University of Southern California, 2017.

36. Kahn, Antoine. "Fermi level, work function and vacuum level." *Materials Horizon* (2016): 7-10.

37. Masafumi Harada and Syoko Kizaki "Formation Mechanism of Gold Nanoparticles Synthesized by Photoreduction in Aqueous Ethanol Solutions of Polymers Using In Situ Quick Scanning X ray Absorption Fine Structure and Small-Angle X ray Scattering" *Nara* 630-8506,

38. Friedrich, R.; Stefan, H.(2005). Photoemission spectroscopy—from early days to recent applications. *New Journal of Physics*, 7 (1), 97.

39. McNeillie, A., Brown, D. H., Smith, W. E., Gibson, M, & Watson, L. (1980). X-ray photoelectron spectra of some gold compounds. *Alistair McNeillie Donald H Brown W Ewen Smith Martin Gibson Lewis Watson*, 767-770.

40. F. Sloan Roberts, S. L. A., Arthur C. Reber, and Shiv N. Khanna. (2015). Initial and Final State Effects in the Ultraviolet and Xray Photoelectron Spectroscopy (UPS and XPS) of Size-Selected Pdn Clusters Supported on TiO2(110). *The Journal of Physical Chemistry C*, 6033–6046.

41. Sorrell, C. C., Nowotny, J., & Sugihara, S. (2005). *Materials for Energy Conversion Devices*: Elsevier Science.